Saturn kilometric radiation periodicity after equinox

G. Fischer [a,*], D.A. Gurnett [b], W.S. Kurth [b], S.-Y. Ye [b], J.B. Groene [b]

[a] *Space Research Institute, Austrian Academy of Sciences, Schmiedlstr. 6, A-8042 Graz, Austria*
[b] *Department of Physics and Astronomy, The University of Iowa, 203 Van Allen Hall, Iowa City, IA 52242, USA*

ABSTRACT

The rotation period of Saturn's magnetosphere was found to vary with time, and changing periodicities were identified in magnetic fields, radio emissions, and charged particles. Here we analyze the varying period of Saturn kilometric radiation (SKR) from 2009 to early 2013, i.e. mainly after Saturn equinox of August 2009. A periodicity analysis is first applied to the complete SKR signal, and second to SKR intensities separated by spacecraft latitude and wave polarization, attributed to SKR from the northern and southern hemisphere. Our analyses are done with the tracking filter approach of Gurnett et al. (Gurnett et al. [2009a]. Geophys. Res. Lett. 36, L16102) and by simply tracing the phases of normalized SKR intensity maxima (north and south) with time. It is shown that SKR periods from the northern and southern hemisphere converged during 2009, crossed shortly after equinox, and coalesced in spring 2010. We will show that SKR from both hemispheres not only exhibited similar periods, but also similar phases from March 2010 until February 2011 and from August 2011 until June 2012. The in-between time interval (March to July 2011) shows a slowdown of the southern SKR rotation rate and a slight increase in rotation speed for the northern SKR before rotation rates and phases become equal again in August 2011. We also identify SKR signals where the modulation phase deviation exceeds one rotation each time Cassini completes one orbit, i.e. this is consistent with the characteristic of a rotating signal. However, the main SKR modulation signals from 2009 to 2012 can be viewed as being clock-like with no correction needed for the derived periods. A comparison of SKR periodicities after equinox to the planetary period oscillations of the magnetic field shows major differences, and we compare SKR phases to magnetic field phases to explain the deviations.

© 2015 Elsevier Inc. All rights reserved.

1. Introduction

Saturn kilometric radiation (SKR) was first detected by the Voyager 1 spacecraft while approaching Saturn (Kaiser et al., 1980), during which its modulation period was determined by Desch and Kaiser (1981) as 10 h 39 min 24 ± 7 s (10.6567 h). The frequency range of SKR goes from a few kHz to 1.2 MHz with peak emission frequencies around a few hundred kHz. SKR is believed to be generated by unstable electron distributions in the auroral zones via the cyclotron maser instability, and it is radiated preferentially in the extraordinary (X) mode. This implies that SKR is mostly right-hand polarized when observed from the northern hemisphere, and left-hand polarized when observed from the southern hemisphere (Kaiser et al., 1984). The period of 10 h 39 min 22.4 s (10.6562 h), which is within the error bar of the Desch and Kaiser (1981) Voyager radio period, was later adopted as Saturn's internal rotation period linked to the planetary

magnetic field (Davies et al., 1996). This definition is based on two assumptions, first that the motion of electrons responsible for the SKR generation is controlled by the planetary magnetic field, and second that the external planetary magnetic field is rigidly linked to the deep interior of Saturn. The second assumption is most likely not true, since observations by Ulysses and the Cassini spacecraft (Galopeau and Lecacheux, 2000; Gurnett et al., 2005) have shown that the SKR period is time-variable and varies of the order of ∼1% over the years. Such a change is far too large to arise from a change in the rotation of the deep interior due to Saturn's massive moment of inertia. Furthermore, Cassini observations have revealed that magnetic field perturbations exhibit a time-variable periodicity as well with a quasi-uniform equatorial field rotating near the SKR period (Andrews et al., 2008, 2011, 2012).

From 2004 until early 2009 SKR had shown two periods of 10.8 h and 10.6 h (Kurth et al., 2008), attributed to SKR radiated from the southern and northern hemisphere, respectively (Gurnett et al., 2009a). The periods converged during 2009 and in spring 2010, about half a year after Saturn equinox of August

2009, the SKR periods from southern and northern hemisphere coalesced around 10.7 h (Gurnett et al., 2010). (Our new interpretation in this paper is slightly different with northern and southern periods already crossing in late August 2009, but also coalescing in spring 2010.) A north–south difference in rotation rate was also found for the 5-kHz Saturn narrowband emissions (Ye et al., 2010) and for the auroral hiss radio emissions with periods similar to SKR in the respective hemisphere (Gurnett et al., 2009b).

Periodicities similar to SKR also appear in magnetic field oscillations (Espinosa and Dougherty, 2000; Espinosa et al., 2003a; Andrews et al., 2011, 2012), the flux of energetic electrons (Carbary et al., 2009, 2011), low energy plasma (Gurnett et al., 2007), energetic neutral atoms (Paranicas et al., 2005), and in the motions of the auroral oval (Nichols et al., 2008). Magnetic field oscillations and energetic electrons even have a time-varying double-periodicity like SKR, and so far it is not known what causes the time variability. It has been suggested that a rotating magnetic cam field structure (Espinosa et al., 2003b; Southwood and Kivelson, 2009), the tilt of the current sheet (Khurana et al., 2009), or a centrifugally driven convective instability in the equatorial plasma disc of Saturn's inner magnetosphere (Gurnett et al., 2007; Goldreich and Farmer, 2007) are responsible for the radio emission modulation. Rotating field-aligned current systems, whether modulated by a magnetic cam or by the inner region of the plasma disk, are a common feature of most models. The currents are aligned with Saturn's magnetic field, and they close in the plasma disc and in Saturn's ionosphere, thereby linking the magnetosphere to the conductive part of Saturn's upper atmosphere. The rotation of the magnetosphere is maintained by the torque exerted by neutral-ion collisions in the upper atmosphere, and the torque is transmitted to the magnetosphere by these field-aligned currents (Huang and Hill, 1989). A changing neutral wind in the auroral ionosphere should therefore have an influence on the slippage of the magnetosphere (Smith, 2006). The field-aligned currents could be influenced by seasonal changes in wind speeds or Pedersen conductivities in the ionosphere, which might cause the temporal variability of SKR periods (Gurnett et al., 2009a). A recent model by Jia et al. (2012) suggests that the field-aligned currents are created by double vortices in Saturn's auroral ionosphere on one or both hemispheres (~1000 km above the 1 mbar level). This new model successfully reproduced many features (rotating magnetic field and mass density perturbations, periodic plasmoid releases, periodic oscillations of magnetospheric boundaries, current sheet flapping, modulation of plasma sheet thickness, periodic modulation of field-aligned currents linked to SKR) of the magnetosphere (Jia et al., 2012) and the magnetotail (Jia and Kivelson, 2012). However, the model does not explain the origin of the postulated double vortex in the auroral ionosphere, and Smith (2014) suggested neutral vortices in the upper stratosphere as plasma and neutrals in the polar ionosphere were observed to be subcorotational.

In Section 2 we will first show the modulation of the complete SKR signal, and in Section 3 we will separate the SKR by its polarization to derive the periods of the northern and southern SKR. In Section 3 we will analyze the SKR by the tracking filter approach of Gurnett et al. (2009a), whereas in Section 4 the periods are derived by simply following the phases of normalized SKR intensity maxima (north and south) with time. We will find that both analyses yield consistent results. Section 5 is devoted to how the nature of SKR as a clock-like or searchlight-like (rotating) radio source influences the SKR phase. In our discussion of Section 6 we compare the SKR modulation to the magnetospheric planetary period oscillations derived from magnetic field data by Provan et al. (2013). Section 7 consists of the conclusions. In the Appendix we outline the tracking filter analysis technique, the separation of SKR by

spacecraft latitude and wave polarization, the tracing of the SKR phases, and the tracing of the magnetic field phases by the method of Andrews et al. (2012).

2. Modulations of the complete SKR signal

The normalized peak-to-peak power of SKR is calculated with a method called tracking filter analysis, which was thoroughly described by Gurnett et al. (2009a, 2011). A short summary of the method is given in Appendix A of this paper. Until early 2010 the SKR modulation spectrogram of the complete SKR signal in Fig. 1 shows two components. The stronger one has a period of ~10.8 h from 2004 until 2009, and it is attributed to SKR originating from the southern hemisphere (Gurnett et al., 2009a). The second component related to northern SKR has a faster period of ~10.6 h (note that both periods should be present in the complete SKR signal). From 2009 on both periods seem to converge until they become approximately equal in early 2010 about half a year after Saturn equinox in August 2009. A reversal of SKR periods was possibly observed by the Ulysses spacecraft half a Saturn year earlier, when the periods seemed to cross about 9 months after the November 1995 equinox (Gurnett et al., 2010). The northern and southern SKR period cannot be distinguished in the large spectral feature present in Fig. 1 modulation spectrogram during most of the year 2010. With the exception of spring 2011, it looks like only one SKR period is present in Fig. 1 until early 2013. We note that Fig. 1 shows the SKR modulation spectrogram until late 2013, but in this paper we focus our analysis on the 4 years from 2009 until the end of 2012.

Equatorial orbits of Cassini are advantageous for the simultaneous detection of SKR from both hemispheres. Beyond the equatorial shadow (from ~$4R_S$ outward, Lamy et al. (2008a)) SKR originating from both the northern and southern hemisphere can almost always be observed. This has led to the strong SKR modulation signal after equinox in Fig. 1. The first two high-latitude excursions of Cassini in 2006/2007 and from early 2008 until mid-2009 (see top panel of Fig. 2) were characterized by long passages of Cassini through the northern hemisphere with only short dips into the southern hemisphere. This has led to a weaker SKR modulation signal for the southern hemisphere during those periods (see Fig. 1) since southern SKR is much less likely observed when Cassini is situated in the northern hemisphere. The absence of the northern SKR modulation signal from 2004 until mid-2006 is discussed in the next section.

3. Analysis of the SKR modulation with respect to hemispheres

SKR is a beamed emission that has its largest intensity from sources located in the post-dawn sector peaking around 08 LT (Lamy et al., 2009). It is thought to be emitted in the extraordinary (X) mode (Kaiser et al., 1984), and its wave polarization should be fixed close to the source region (Lamy et al., 2011). The SKR beaming is in such a way that for sources located in the northern hemisphere the angle between the wave vector and the magnetic field is less than 90°, yielding X-mode SKR that is right-hand polarized. For sources located in the southern hemisphere this angle is larger than 90° so that X-mode SKR must have left-hand polarization. Thus, SKR polarization is a practicable means with which the hemispheric origin of SKR can be determined. There is also some ordinary (O) mode SKR with opposite polarization compared to X-mode SKR, albeit with O-mode flux densities typically ~10^4 times lower than X-mode SKR (Cecconi et al., 2009). This means that the integrated intensities of O-mode SKR in our tracking filter analysis should be negligible. The latitude of the observer is crucial for the visibility of the northern and southern sources (Kaiser et al.,
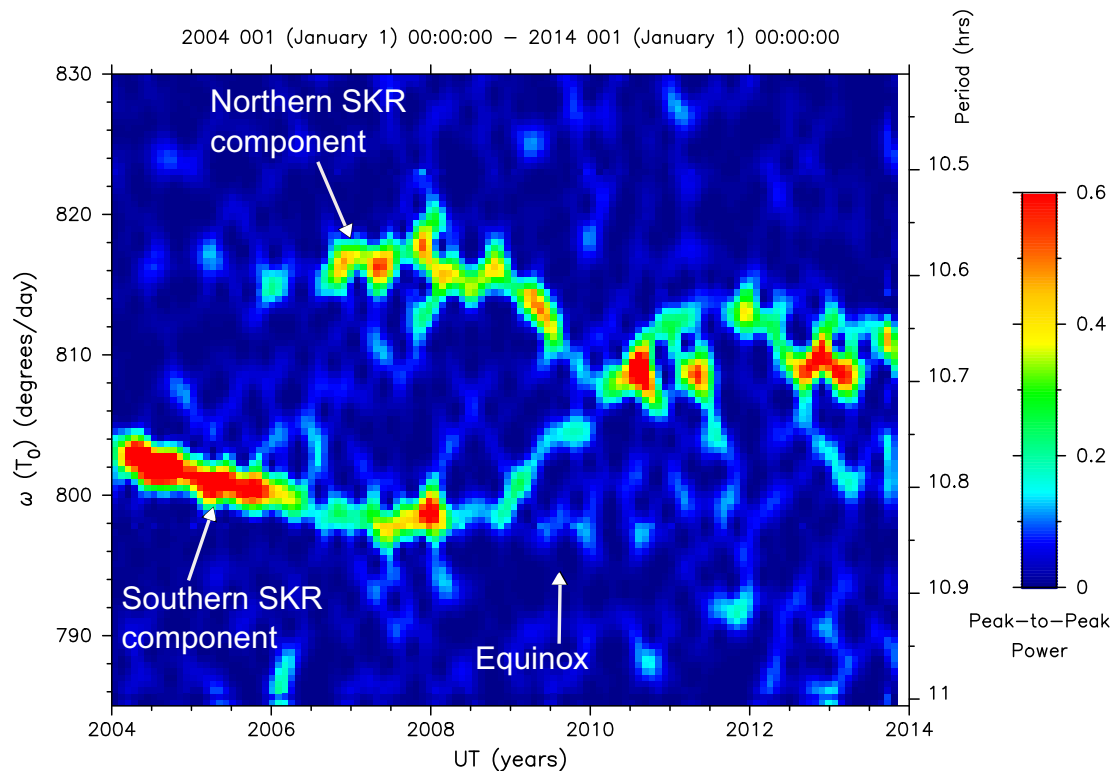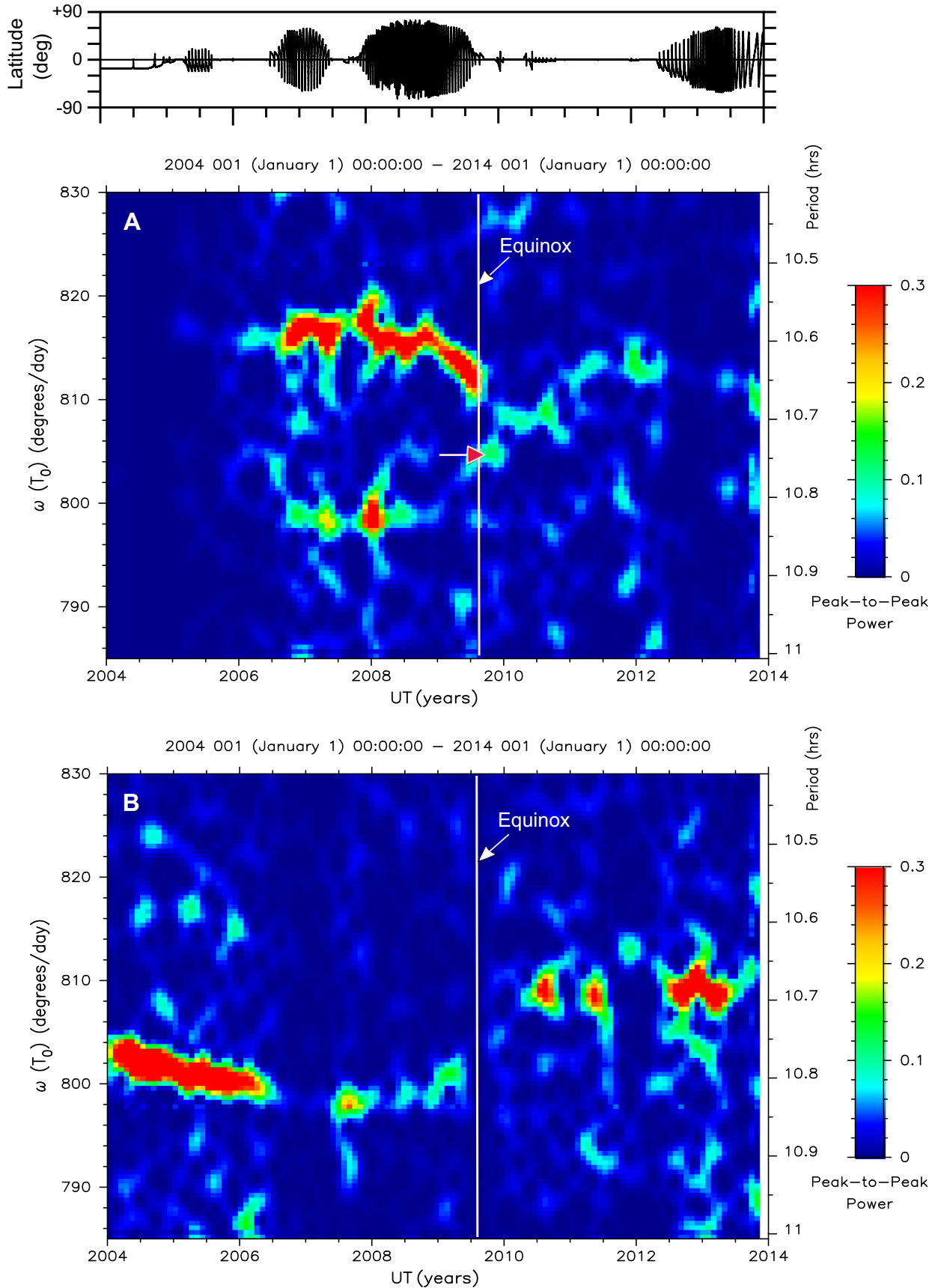
Fig. 1. Normalized peak-to-peak power of Saturn kilometric radiation modulation as a function of time from 2004 until late 2013. The ordinates show the angular velocity (rotation rate) in degrees per Earth day (left side), and the corresponding rotation period in hours (right side). The normalized peak-to-peak power is given by the color bar, and the signal processing was done as in Gurnett et al. (2009a). There are two periods related to SKR from different hemispheres until shortly after equinox, but there is mainly one period from early 2010 until early 2013 except for a few months in early 2011. There seem to be two periods again (~808°/day and ~812°/day) in the first half of the year 2013. (For interpretation of the references to color in this figure legend, the reader is referred to the web version of this article.)

1984; Lamy et al., 2008b; Kimura et al., 2013). Right-hand polarized SKR originating from northern sources can be observed from 20°S up to high northern latitudes. Left-hand polarized SKR originating from southern sources can be observed from 20°N down to high southern latitudes. This symmetrical behavior has been shown by Lamy et al. (2008b), and it suggests that an observer in the equatorial plane can observe the northern and southern SKR equally well beyond the equatorial shadow zone (Lamy et al., 2008a). The equatorial trajectory of Cassini from autumn 2009 until mid-2012 (see top panel of Fig. 2) has ensured a similar visibility for northern and southern SKR in this time interval. When radio waves from both SKR sources reach the RPWS antennas simultaneously there is an incoherent superposition of oppositely polarized waves, where the polarization sense is determined by the stronger SKR component. In Appendix B of this paper it is described in detail how SKR intensities are separated by both circular polarization and spacecraft latitude, in a method which is somewhat different to those of Lamy (2011) and Gurnett et al. (2009a). Our method allows a determination of both northern and southern SKR intensities for each single time–frequency measurement, eliminating the problem of obscuration of weaker SKR by stronger SKR from the opposite hemisphere.

The modulation spectrogram of Fig. 1 has been calculated with the complete SKR signal, without any separation by polarization or spacecraft position. In the following Fig. 2 two modulation spectra are obtained since the SKR intensities of both hemispheres were integrated separately, and the tracking filter analysis was applied to both of them. Fig. 2A shows that before Saturn equinox the northern SKR had a period of ~10.6 h (or ~815°/day), and Fig. 2B shows that at the same time the southern SKR period was ~10.8 h (or ~800°/day) (Gurnett et al., 2009a). The separation by

polarization seems not completely clean since the southern period of ~10.8 h can also be discerned in the northern SKR spectrogram of Fig. 2A, especially from autumn 2006 until mid-2008. Lamy (2011) suggested that the secondary peak at ~10.8 h in the northern signal is likely to reflect a real physical dual modulation. He argues that SKR sources have been identified on closed field lines and that auroral electrons accelerated in one hemisphere can ultimately reach the other one. This interesting idea actually means that one hemisphere does not always have just a unique period, but that a secondary period corresponding to the period of the other hemisphere can also be present in the SKR signal. Fig. 2A shows *two* northern periods from autumn 2006 until mid-2008. The faster signal at a rate around 817°/day is the primary northern signal, which is stronger than the secondary signal around 798°/day. The secondary signal may be caused by periodic bunches of electrons originating from the southern hemisphere which are transformed to SKR radiation above the northern aurora from where right-hand polarized radio waves are emitted. However, there are other possibilities by which such a secondary signal could be created. The first is that the visibility of the SKR sources along one Cassini orbit is modulating the normalized SKR amplitude. If there is a certain regularity of Cassini orbits (as it is the case for part of 2007 when the northern SKR shows a strong secondary signal), one gets a signal whose amplitude is regularly modulated by the Cassini orbit resulting in two side bands of smaller amplitudes. (A tracking filter analysis over an increased rotation rate interval does indeed show another weaker side band also at higher rotation rates for the year 2007; not shown here.) The sidebands are at the frequencies $f \pm f_{orbit}$ with f being the frequency (rotation rate) of the main modulation signal and f_{orbit} as the orbital frequency of Cassini. These sidebands can also be viewed as the orbital

Fig. 2. Normalized peak-to-peak power of northern and southern SKR modulation as a function of time from 2004 until late 2013. The display is similar to Fig. 1, but here SKR is separated by polarization with northern SKR in panel A and southern SKR in panel B. We also show the planetocentric latitude of Cassini above panel A. The vertical white lines indicate Saturn equinox of 11 August 2009. The red-headed arrow denotes a spectral feature shortly after equinox which is explained in the text of Section 3. (For interpretation of the references to color in this figure legend, the reader is referred to the web version of this article.)

alias frequencies for $n = ±1$ which are given by the formula $f_{alias} = |f − n · f_{orbit}|$ with n being an integer number.

In general, the strength of the modulation signals in Figs. 1 and 2 depends on parameters like the spacecraft latitude and local time that influence the SKR visibility, the presence of radio emissions within the analysis window, and the radio emission's intensity. The absolute SKR intensity has probably only a minor influence as long as it is intense enough for detection. This is due to the normalization procedure in which the integrated SKR intensity is divided by the average intensity over one Saturn rotation (see Appendix A). Visibility effects and the variation of SKR intensity with local time cannot be mitigated by the normalization procedure. The strength of the modulation signals is also low in case of rapid frequency variations and when the received radio emissions simply lack a stable periodicity over the 240 day window leading to low spectral amplitudes. The latter could be the reason why the northern SKR modulation signal has only a modest intensity in the first two years after equinox (see Fig. 2A) compared to the southern SKR modulation signal (Fig. 2B) despite the similar hemispheric SKR visibilities due to the equatorial trajectory. Starting in 2010, the major strong modulation signals of SKR come from the southern hemisphere with one relatively intense feature in each year from 2010 to 2012 (the last one also reaching into 2013). Before equinox, the strength of the southern SKR modulation signal can be well explained with the changing SKR visibility caused by Cassini's latitude. The southern SKR modulation signal is weak from mid-2006 until mid-2007 and from spring to autumn 2008. These time intervals correspond to high latitude orbits of Cassini that are characterized by long passages through the northern hemisphere and only short dips into the southern hemisphere. Only a certain interval of the second Cassini high-latitude excursion from autumn 2008 until spring 2009 is characterized by orbits with about equal dwell times in the northern and southern hemisphere, and it is in that interval where the southern SKR modulation signal is stronger. However, the Cassini trajectory cannot explain the practically absent southern SKR modulation signal from mid-2009 until early 2010 since Cassini was mostly in the equatorial plane during this time. The absence of the northern SKR modulation signal from 2004 until mid-2006 can partly be explained by Cassini's southern latitude, but also the conditions for the generation of SKR in the north were non-favorable during this time. A comparison of absolute SKR intensities between northern and southern hemisphere was done by Kimura et al. (2013). They showed high southern SKR intensities during southern summer conditions and only sparse northern SKR until late 2005.

The time interval right after Saturn equinox on 11 August 2009 (indicated by a vertical white line in Fig. 2) is also highly interesting. We can see a moderately intense northern SKR modulation signal in Fig. 2A at 804°/day which is marked by a red-headed arrow. There are only very weak southern SKR modulation signals for about half a year after equinox from which the correct period cannot really be determined. Since the northern SKR signal makes a jump down to 804°/day right around equinox, it is possible that northern and southern period cross some time between equinox and the beginning of 2010. We will show that this is actually the case in the next section. Looking at the complete SKR modulation signal of Fig. 1, one would rather attribute the signal at 804°/day (10.746 h) from late 2009 as belonging to the southern SKR component due to its proximity to the southern SKR period, which is the interpretation of Gurnett et al. (2010) and Lamy (2011). Similarly, in Fig. 1 there is a connecting signal leading from ∼811°/day at equinox down to ∼808°/day at the end of 2009 which seems to connect the strong northern signal of early 2009 with the large spectral feature of 2010. However, the modulation spectra of SKR separated by polarization show a different picture. The right-hand polarization of the signal at 804°/day should ensure that the radio

waves originate from sources in the northern hemisphere. Could it be possible that this signal at 804°/day is a secondary signal caused from electrons coming from the other hemisphere? This possibility is unlikely, because there are no strong primary signals of southern and northern hemisphere despite the similar visibility of southern and northern hemisphere due to the equatorial Cassini trajectory. Therefore we conclude that the northern SKR rotation rate jumps down from 812°/day to 804°/day shortly after equinox. The tracing of the SKR phases in the next section will also support this conclusion.

We note that Fig. 2 shows two periods again in the year 2013. The modulation signal of northern SKR is absent for about one year from early summer 2012 until early summer 2013, after which a weak signal can be seen around 812°/day. The southern SKR has a different rotation rate of 809°/day around the same time in mid-2013. By autumn 2013 both rates are again close to each other around 810°/day. This behavior will be analyzed in a future paper, and here we focus our analysis on the years 2009 until the end of 2012.

4. Tracing the phase of SKR maxima

4.1. Phase drift of normalized SKR intensities organized by constant guide period

The Lomb-Scargle analysis technique used by Lamy (2011) and the tracking filter analysis of Gurnett et al. (2009a, 2010, 2011) employed here use sliding windows lasting longer than 3 months (here we use 240 days). However, it is known that the phase and period of SKR can also exhibit short-term changes on a timescale of weeks that are attributed by Zarka et al. (2007) to the external influence of the solar wind speed. We can gain further insight into the SKR modulation by simply following the SKR phase as a function of time which should allow us to see changes on shorter timescales (Kurth et al., 2007). In the following we investigate the phase drift of the northern and southern SKR intensities relative to a fixed period as a function of time from the beginning of 2009 until the end of 2012. A concise mathematical description of this procedure is given in Appendix C. In Fig. 3 we employ a constant guide period of 10.6567 h (for both northern and southern SKR), which is arbitrarily chosen as identical to the Voyager radio period of Desch and Kaiser (1981). There is no artificial phase shift introduced between northern and southern SKR phase, and we arbitrarily set the guide phase to +90° at $t = 0$ at 00:00 SCET on January 1, 2004 (beginning of day), i.e. we use DOY (day of year) 2004 as our time counter.

Panels A and C of Fig. 3 show the phase drift of the northern SKR as a function of time for two years each, which are 2009–2010 and 2011–2012, respectively. Similarly, panels B and D show the normalized intensities of the southern SKR as a function of time and phase. Similar plots have been made by Kurth et al. (2007, 2008) for the complete SKR signal (not separated by hemisphere) before equinox. For the northern SKR there are gaps (regions with no SKR intensity where the ratio indicated by the color bar was set to zero) in the beginning of 2009 and the end of 2012 (panels A and C) which is simply due to the restriction to latitudes above 20°S, since no northern SKR is usually detected at high southern latitudes. Similarly, some gaps are also present around the same time for the southern SKR (panels B and D) since Cassini was at high northern latitudes in these parts of the high-inclination orbits. Two real major data gaps were in the first half of November 2010 (after day 2500) and at the end of October 2012 (around day 3220) when no RPWS data were taken for several days.

In Fig. 3 the phase is plotted over two rotations (720°) to enable a better tracing of the SKR intensity maxima. The white and red lines track those maxima for northern and southern SKR phases,
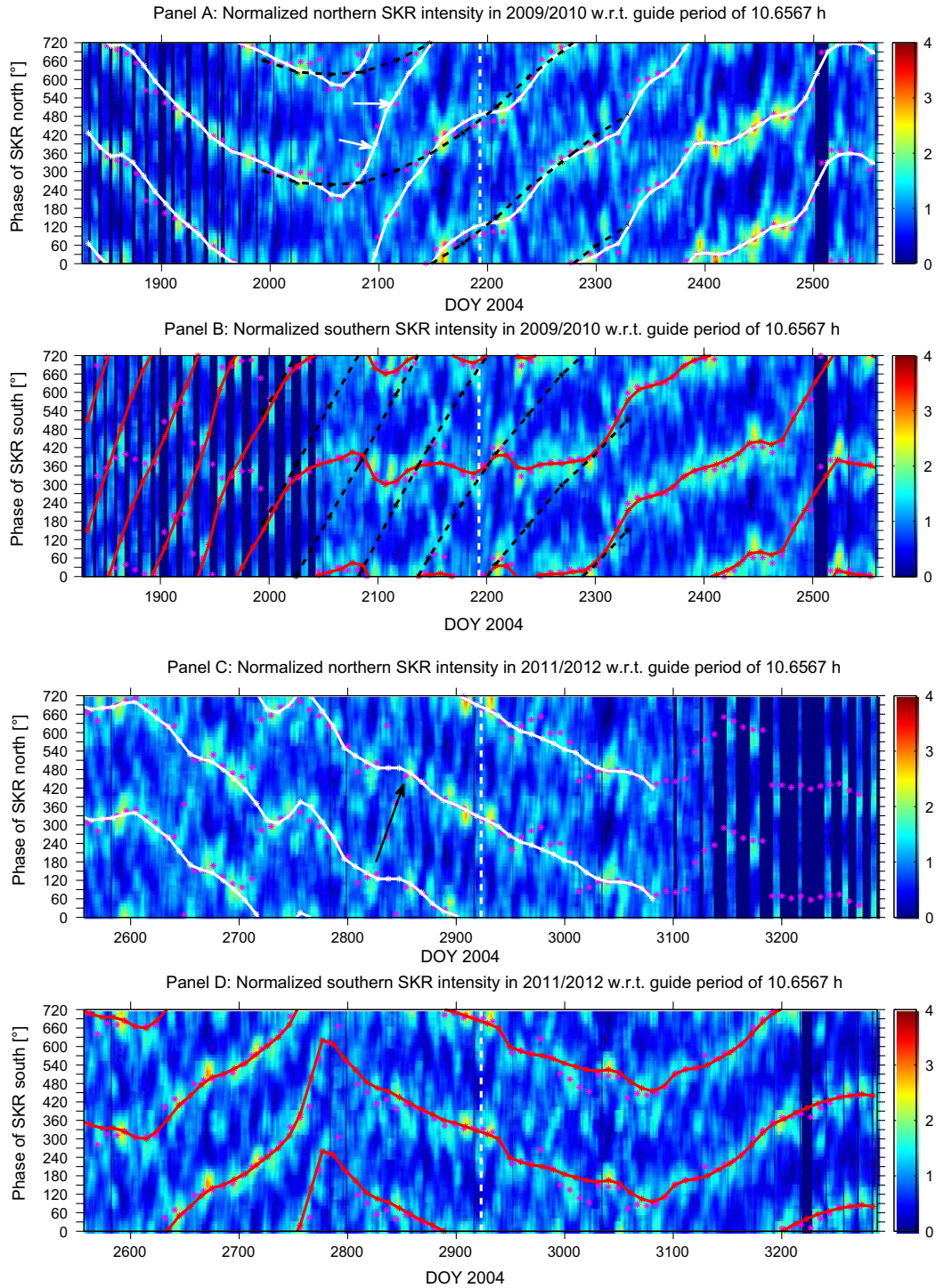
Fig. 3. Phase drift of northern and southern SKR intensities with respect to a constant guide period of 10.6567 h over 4 years. Panel A shows the phase drift of the northern SKR with respect to a constant guide period of 10.6567 h versus time for the two years 2009 and 2010. This is continued in the third panel C, where the phase drift of northern SKR can be followed over the two years 2011 and 2012. The second panel B shows the phase drift of the southern SKR with respect to the same constant guide period of 10.6567 h versus time for the two years 2009 and 2010, and panel D shows the same for the years 2011 and 2012. The time is given in days of year (DOY) 2004 from 1827 to 3288 (January 1, 2009, until beginning of January 1, 2013), and the white vertical dashed line in each panel separates the year 2009 from 2010 (panels A, B) and 2011 from 2012 (panels C, D). The intensities (north and south) are normalized by dividing them by the averaged SKR intensity over one rotation (360°), and this ratio r is color-coded according to the color bar on the right side. The SKR intensity ratios are averaged for guide phase intervals of 10° (corresponding to ~18 min), yielding 36 values per rotation. These values are plotted twice over 720°, allowing an easy tracing of the phases. To enhance the visibility of the SKR maxima, the whole 2D matrix of SKR intensity ratios was smoothed. (This was done by replacing each value r of the SKR intensity ratio by the mean over a rectangle of 70° and 17 rotations centered on r.) The white lines of panels A and C have been inserted to trace the northern SKR maximum values with one data point every 10 days. Similarly, the red lines of panels B and D trace the maxima of the normalized southern SKR intensities. The magenta stars were calculated with directional statistics (see Appendix C) to help tracing the SKR phase maxima (close to white and red lines). The dashed black lines in panels A and B show the maxima of the SKR phases as they should be when the rotation rates of Lamy (2011) and Gurnett et al. (2010) are taken. The two white arrows in panel A indicate two specific SKR maxima which are mentioned in the text. The black arrow in panel C is discussed in the text, and it indicates an alternative way of following the SKR maxima which we consider as less likely.
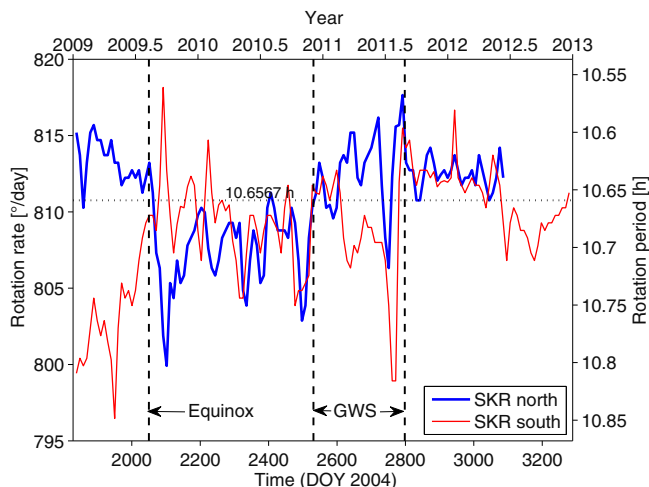
Fig. 4. Rotation rates (in °/day) of SKR over 4 years from the beginning of 2009 until the end of 2012. The SKR rates have been derived by following the SKR phases of Fig. 3. (The rotation rates are the temporal derivatives of the phases, see Appendix C.) They are displayed as solid lines in blue and red color for northern and southern SKR, respectively. The lower horizontal axis denotes the time in DOY 2004, and the upper horizontal axis shows the time in years. The left vertical axis shows the rotation rate in degrees per day, whereas on the right one can see the rotation period in hours. The horizontal dotted black line indicates the constant guide period of 10.6567 h (810.7576°/day). The black dashed lines indicate the time of Saturn equinox (August 11, 2009), and the start and end of the Great White Spot (GWS) event (December 5, 2010 until August 28, 2011), respectively. (For interpretation of the references to color in this figure legend, the reader is referred to the web version of this article.)

respectively. They were drawn by hand with one data point every 10 days, but guided by the magenta stars which were calculated by directional statistics. The employed mathematical procedure, which aims at finding the phase of the SKR maxima, is described in Appendix C. One can see that the hand-drawn white and red lines generally follow the calculated magenta stars very closely. The phase at the northern SKR maxima has mainly a negative slope from the beginning of 2009 until autumn 2009 and from early 2011 until mid-2012 (except around day 2750). This means that the period τ_n is smaller (faster) than the constant guide period, i.e. $\tau_n < 10.6567$ h. Sometimes the slope of the white line is around zero, which means that here the northern SKR period is equal to the constant guide period of 10.6567 h (or ~810.76°/day). The positive slope of the white line from autumn 2009 until the end of 2010 indicates a northern SKR period that is larger (slower) than the guide period, i.e. $\tau_n > 10.6567$ h. The white line has not been drawn further than day 3086 (mid-June 2012) since Figs. 2A and 3C show no clear northern SKR signal afterwards. This is mainly due to Cassini's trajectory which goes again to higher latitudes, but this time with long excursions through the southern hemisphere and very short dips into the northern one (see top of Fig. 2). The phase drift for the southern SKR in panels B and D of Fig. 3 has mostly positive slopes, i.e. there is $\tau_S > 10.6567$ h. The slope is clearly negative from August/September 2011 to May/June 2012.

4.2. SKR periods and phases

Since the slope of the phase tracing the SKR maximum indicates the rotation rate (see Appendix C), one can clearly see in Fig. 4 when the rotation rates are above and below the guide period of 10.6567 h indicated by the horizontal dotted line. In Fig. 4 we have drawn the rotation rates of northern and southern SKR as a function of time over 4 years. The rotation rates are calculated by temporal derivatives of the underlying phases curves after Eqs. (6) and (7) in Appendix C, whose errors are given by the uncertainty of the

slopes of the white and red lines in Fig. 3. The rotation rates in Fig. 4 show many short-term changes due to the temporal resolution of 10 days with which the SKR phases at the maxima are traced. In the tracking filter analysis technique they are averaged out by the usage of long (240 days) windows.

Fig. 4 shows that northern and southern SKR periods already crossed in late August 2009, shortly after equinox, with equinox being indicated by the vertical dashed line. This result is consistent with our previous tracking filter analysis, but different to Gurnett et al. (2010) and Lamy (2011) who suggested that northern and southern periods coalesce or cross in spring 2010, about 7–8 months after equinox. For comparison we have taken their suggested rotation rates and calculated the respective phase maxima for northern and southern SKR by integrating over their rotation rates. The integration constant was set to a value with which we arrive at the same values for their and our phase maxima around day 2000 (late June 2009). The black dashed lines in panels A and B of Fig. 3 from June 2009 until May 2010 are the values for the SKR phases based on the interpretation of Gurnett et al. (2010) and Lamy (2011). For the northern hemisphere we can argue that our white line looks like the best match to the SKR maxima. It goes through both SKR maxima indicated by the two white arrows, the first one around day 2090 at 360° (equivalent to 0° and 720°), and the second one around day 2110 at 540° (equivalent to 180°). The dashed black line does not go through any of these maxima. Note that our directional statistics (magenta stars) also follows our white line. For the southern hemisphere the better match of our red line to the SKR maxima is even more obvious since the dashed black line goes through a lot of "empty" blue area away from the most intense southern SKR maxima. However, there are still some southern SKR signals around the black dashed lines (e.g. magenta stars at ~420° around day 2150), and it is interesting that they are at similar times and phases like the northern SKR signals, which can be seen by a careful comparison of Fig. 3B with Fig. 3A. It looks as if the southern SKR phase would try to follow the northern SKR phase for some days before jumping back in phase due to its own faster period. This behavior might cause the weak secondary signal in the southern SKR modulation spectra
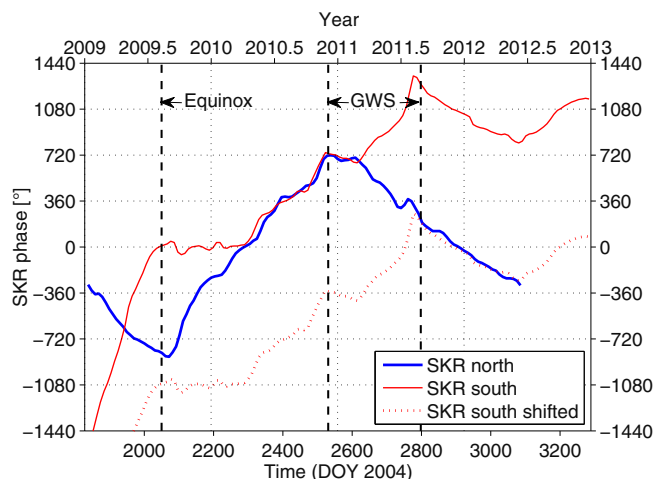
Fig. 5. Phases of northern and southern SKR maxima with respect to the constant guide period of 10.6567 h, plotted over 8 rotations. The plot goes from the beginning of 2009 until the end of 2012 with years separated by vertical dotted lines and indicated on the top. The display allows seeing when the phases of northern (blue line) and southern SKR (red lines) are very similar. Their difference is small (within 100°, but mostly less) from days 2270–2610 (mid-March 2010 to mid-February 2011) and from days 2780 to 3080 (mid-August 2011 to early June 2012). The vertical black dashed lines indicate the time of Saturn equinox (August 11, 2009), and the start and end of the Great White Spot (GWS) event (December 5, 2010 until August 28, 2011), respectively. (For interpretation of the references to color in this figure legend, the reader is referred to the web version of this article.)

around the northern period of 804°/day in late 2009 (see Fig. 2B and later the lower panel of Fig. 6). Nevertheless, the main southern SKR intensities from day 2050 (equinox) until 2300 are still clustered around a constant phase around 360°, suggesting a period similar to the guide period, but with large variations due to the short-term oscillations/jumps of the phase maxima. The northern and southern SKR phases approach each other again some days before day 2300 after which their phases finally seem to get locked leading to similar periods. This behavior can be expected under the assumption that ionospheric conductivities and winds (Gurnett et al., 2009a; Jia et al., 2012) play a role in establishing the periods. Ultimately, similar conditions in both hemispheres around equinox should lead to similar SKR phases and periods.

We point out the positive slope of the northern SKR maxima a few days around day 2750 (July 2011) that is drawn as a white line in Fig. 3C. The rotation rate of the northern SKR is difficult to determine around that time since no northern modulation signals can be found in Fig. 2A. The way we have drawn the white line is one likely option, since the major northern SKR maxima are followed in this way. There are only a few instances of time when the directional statistics (magenta stars) would indicate another path for the SKR maxima to be taken. One is around day 2840, indicated by the black arrow in Fig. 3C. However, the SKR signals are weak and there is no corresponding signal in the tracking filter analysis. The signals could be rotating SKR signals (see Section 5), and so we preferred to follow the general trend of autumn 2011 with declining northern SKR phases with time. The single magenta star around 360° and day 2650 in the northern SKR intensities (see Fig. 3C) is most likely also due to a minor rotating SKR signal. The southern SKR phase in the first half of 2009 is also difficult to

follow, but we took a path that is consistent with the tracking filter analysis signal around 800°/day.

Fig. 4 shows that for long intervals of time the northern and southern SKR periods are almost identical after equinox. This is the case for a first interval starting in March 2010 and lasting for almost one year until February 2011, and for a second interval from about August 2011 to June 2012. There are actually not only the periods of northern and southern SKR that are similar in these time intervals, also the SKR phases from both hemispheres are similar. (A comparison of phases between northern and southern SKR can only be done when the same guide period is used for both hemispheres.) This can be seen by a careful inspection of Fig. 3, where we have pointed out the start of the phase lock between northern and southern SKR shortly before day 2300 in the previous paragraph. But, it is much easier to see in Fig. 5 where we have drawn the phases of northern and southern SKR as a function of time. It is remarkable that this similarity in SKR periods and phases is interrupted in a time interval from March to August 2011, which is roughly contemporaneous with the occurrence of the so-called Great White Spot (GWS), a major atmospheric disturbance in Saturn's northern hemisphere (Sánchez-Lavega et al., 2011). The GWS of 2010/2011 was a giant thunderstorm with lightning activity measured by the Cassini RPWS instrument from 5 December 2010 until 28 August 2011 (Fischer et al., 2011; Sayanagi et al., 2013). This time interval of the GWS event is indicated in Figs. 4 and 5, and the periods of northern and southern SKR are largely different there except for the first 2–3 months. It is also worth noting that the strong southern SKR modulation signal centered at 808°/day in our Fig. 2B is similar to the 10.69 h rotation period of the GWS head region. The GWS was located at 35° North, which
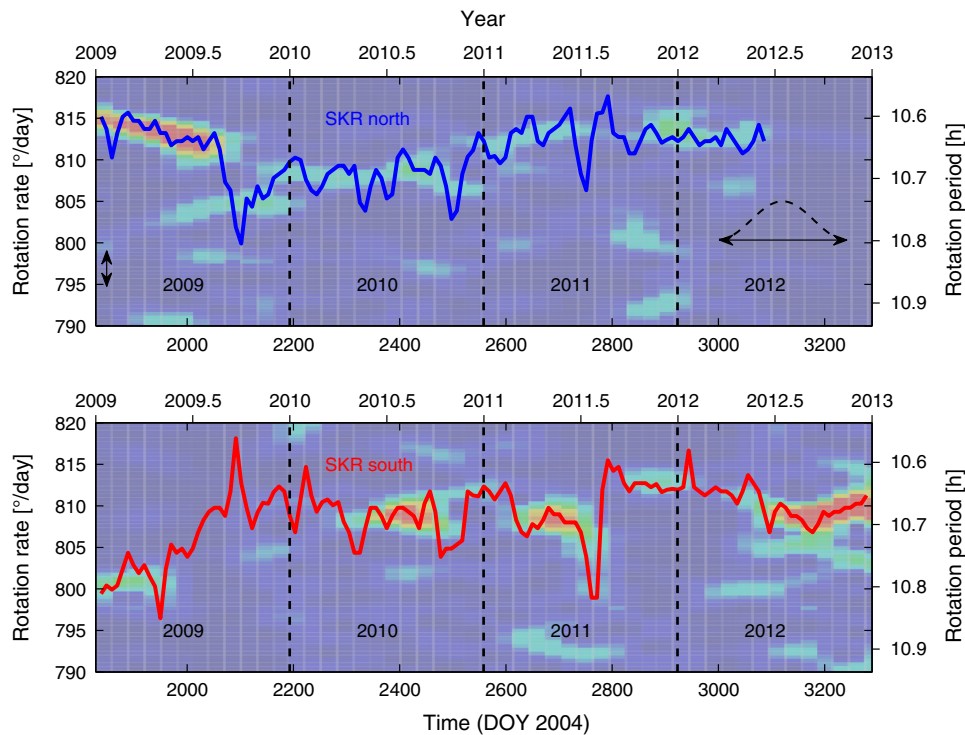
Fig. 6. Rotation rates of northern and southern SKR over 4 years from the beginning of 2009 until the end of 2012 with comparison between results from the tracking filter analysis and from tracing the SKR phase maxima. The horizontal time axes indicate days of year 2004 (bottom axes) and years (top axes). The vertical axes give the rotation rate on the left (in °/day) and the rotation period on the right (in hours). The blue curve in the upper panel shows the rotation rate of northern SKR, and the red curve in the lower panel shows the rotation rate of southern SKR. Both curves were gained from tracing the SKR phase maxima and are identical to the corresponding curves in Fig. 4. In the background one can see the results from the tracking filter analysis, comparable with Fig. 2, but with subdued colors. The black dashed vertical lines are drawn to separate the years from each other. The vertical black double-arrow in the upper panel indicates the variation of the blue and red lines around the tracking filter analysis signals. In the upper panel we also illustrate a 240-day long Hamming window as it was used for the tracking filter analysis. (For interpretation of the references to color in this figure legend, the reader is referred to the web version of this article.)

means that some intermediate process (e.g. global thunderstorm-induced gravity waves in the atmosphere) must be at work to influence the auroral latitudes around 75° which are the magnetic footprint latitudes of SKR. Fig. 5 shows that the GWS is almost contemporaneous with the time interval when the lock-step phasing of the two SKR sources was broken. The breakup happens about 2–3 months after the start of the GWS, which could be due to the temporal inertia of atmospheric processes. We do not further elaborate on this remarkable coincidence in this paper, since this topic is thoroughly discussed in Fischer et al. (2014).

4.3. Comparison of results

The rotation rates derived from tracing the SKR maxima and from the tracking filter analysis are in very good agreement with each other. This can be seen in Fig. 6 where we have drawn the northern and southern rates from Fig. 4 as blue and red line in the upper and lower panel, respectively. The SKR modulation spectrogram of the respective hemisphere from the years 2009 to 2012 is drawn in the background in subdued colors for direct comparison. The northern period experiences a sharp drop from 812°/day to 804°/day in autumn 2009, and the southern period arrives around 810°/day in late 2009. The southern SKR modulation signal of the tracking filter analysis is largely absent from mid-2009 until spring 2010, which might be due to the changing southern SKR phase at the maxima in this time interval according to Fig. 3B. However, the tracing of the southern SKR phase maxima did allow the determination of the southern period in this time interval.

The varying broadness of the SKR modulation signals in Fig. 6 indicates the variability of the rotation rate. The northern SKR modulation signals extend over ±2.5°/day in mid-2009 and in late 2011/early 2012, and the southern SKR signals are even broader in mid-2010, mid-2011, and in the second half of 2012. However, for the rest of the time the signals extend over just ±1°/day. The red and blue lines are often very close to the center of the main SKR modulation signal. Their average deviation can be estimated as within ±2.0°/day, indicated by the black double arrow in the upper panel of Fig. 6. This corresponds to a relative error of ~0.25% or to an error for the period of 0.027 h or ~1.6 min. Only in some cases are there larger deviations due to SKR short-time fluctuations that are averaged out in the long window of the tracking filter analysis. These short-time fluctuations might be real and could be due to the influence of the solar wind on Saturn's radio clock (Zarka et al., 2007). A detailed study between the solar wind properties at Saturn and the SKR phase variations is beyond the scope of this paper and could be the subject of a future study.

The tracing of the phases at SKR maxima can be criticized as being somewhat subjective. However, it was firstly guided by the mathematical method of directional statistics described in Appendix C, and secondly the agreement with the results from the tracking-filter analysis illustrated in Fig. 6 has demonstrated a good agreement. Another way to illustrate the correctness of our derived northern and southern SKR periods is to organize the SKR intensities with respect to northern and southern phase systems based on just these time-variable periods. Therefore, we took the northern and southern rotation rates $\omega_N(t)$ and $\omega_S(t)$ as displayed in Fig. 4 and integrated the two equations (4) of Appendix C to calculate northern and southern phases as a function of time (modulo 360°). The normalized northern and southern SKR intensities are now displayed (over 720°) with respect to these phases
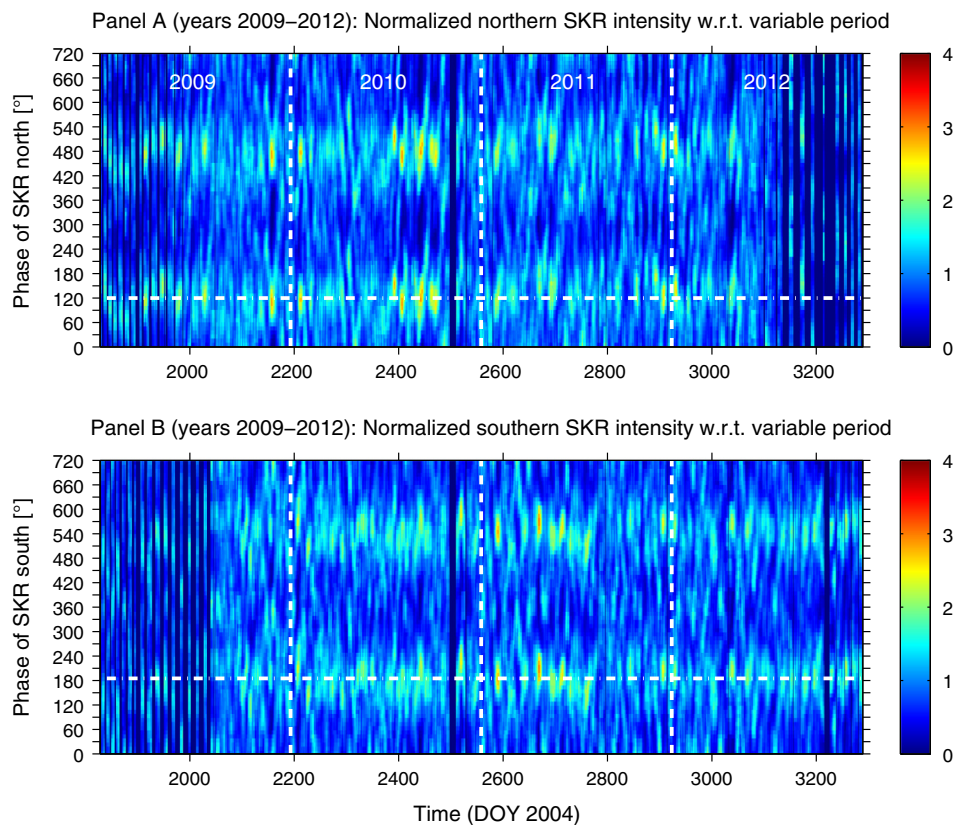

Fig. 7. Plot of normalized northern and southern SKR intensities as a function of time with respect to guide phases with a variable period. Both panels go from the beginning of 2009 until the end of 2012, and the vertical dashed white lines separate the years. We have constructed two phase systems that are based on the variable periods of northern and southern SKR, respectively, as they are displayed in Fig. 4. We arbitrarily set the northern and southern guide phase to zero at the beginning of the first day of 2009. In such systems the SKR maxima should cluster around constant phase values. The horizontal white dash-dotted lines indicate that this is largely the case for both northern (panel A) and southern (panel B) SKR.

in panels A and B of Fig. 7, respectively. This is similar to the organization of SKR data with respect to a time variable longitude system as done by Kurth et al. (2007) in their Fig. 3 or by Kurth et al. (2008) in their Fig. 9. The result of this procedure should be SKR intensity peaks clustered around a constant phase allowing to judge the correctness of the periods. In both panels A and B of Fig. 7 it can be seen that the northern and southern SKR peak intensities are pretty well organized by the horizontal white dash-dotted lines. There only seems to be a certain phase shift for the northern SKR in the second half of the year 2012, where we mentioned that the northern SKR period is uncertain (not drawn in Fig. 4) due to extended dwell time of Cassini in the southern hemisphere. (For the organization of northern SKR data in Fig. 7A for the second half of 2012 we used a northern period equal to the southern one.)

Our SKR periods are largely different to the magnetic field oscillation observations which indicate that the northern and southern period did not cross after equinox according to Andrews et al. (2012) and Provan et al. (2013). We will make a more detailed comparison of SKR and magnetic field rotation rates in Section 6. First we want to discuss a suggestion by Andrews et al. (2011, 2012), that the position of the observer (Cassini spacecraft) could influence the SKR phase. They suggest position-dependent effects in the SKR phase due to the rotation of the SKR modulation around the auroral oval combined with incomplete seeing of the radio sources from Cassini.

5. SKR: A clock-like or a rotating source?

The question if the SKR modulation phase depends on the spacecraft position is linked to the intrinsic nature of the radio source, in particular whether it is a clock-like source or a rotating beacon (also called a "searchlight" in analogy to light from a light house or an aerobeacon). The diagram from Warwick et al. (1981) showing the occurrence probability of SKR before and after the Voyager 1 encounter has been the first and main argument for the clock-like behavior of SKR. The sub-solar longitude ordered the SKR occurrence very well with just one peak, which was taken as evidence that the SKR radiation pattern is fixed in local time relative to the Sun. When plotted versus the sub-spacecraft longitude, there are two histograms of similar shape offset by ~120°, and this shift between the histograms was equal to the angle through which Voyager 1 moved during the Saturn flyby (Gurnett et al., 1981; Kaiser et al., 1984). Only recently, some evidence was presented by Lamy (2011) that SKR sources are also rotating, in contrast to the early Voyager picture of sources fixed in local time. In his Fig. 5a, Lamy (2011) plotted the flux density of southern SKR sources gained from 1% of the data via radio wave direction finding versus source local time and southern SKR phase Φ_S and found a linear relation. In his figure, the dawn-side SKR sources rotate from 0 to 12 LT while the southern phase Φ_S roughly goes from 180° to 360°. SKR sources might also uniformly rotate through the dusk sector, but dusk-side SKR sources are sparse in the data set of Lamy (2011) simply because during that time Cassini was mostly located on the dawn side with limited viewing of SKR from the dusk side. Within the 4 years 2009–2012 studied here the apoapsis of Cassini was mainly on the dusk side, which means that mostly dusk side sources should have been observed. Lamy et al. (2013) showed a bright and longitudinally extended corotating auroral region locked at the SKR phase and that SKR arcs are related to isolated auroral spots. In order to maintain a physical link between the rotating magnetic field and SKR, the SKR sources should also be rotating, similar to the rotating ultraviolet and infrared auroral ovals. However, there are also several images of Saturn's aurora showing illumination of all local times (e.g. see
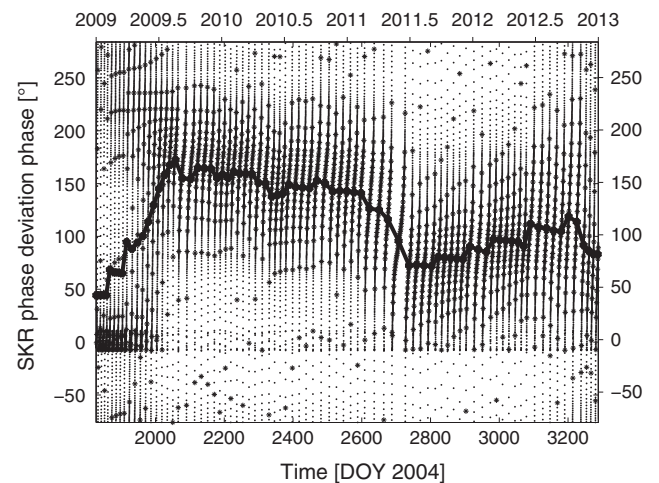

Fig. 8. The SKR phase deviation $\Delta\varphi$ as a function of time from the beginning of 2009 until the end of 2012 calculated using the model of Andrews et al. (2011, their Fig. 2c). Small black dots show $\Delta\varphi$ values for each hour and small black stars for each day. The thick black line connects the orbit-averaged SKR phase deviations. (The daily and orbit-averaged phase deviations are calculated as averages from hourly values.)

Fig. 4 of Bunce et al., 2014) or non-rotating features (e.g. Fig. 3 of Badman et al., 2013), in contrast to the rotating picture of dawn- and duskside sources in anti-phase. This suggests that there might be static as well as rotating current systems. The camshaft model of Southwood and Kivelson (2009) explains how a rotating magnetic field can cause a clock-like SKR signal at a fixed local time. The rotating upward currents generating the rotating SKR signal appear to peak in amplitude just once per rotation period, producing a clock-like signal. The rotating SKR signal is weak except when it reaches the morning side where it intensifies.

5.1. Model of a rotating SKR source

A rotating SKR source would lead to a dependence of the SKR phase on the local time of the observer, as it is shown in Fig. 2c of Andrews et al. (2011). While the spacecraft is making one orbit around Saturn, the SKR modulation phase deviation goes from 0° to 360°, i.e. over one full rotation. The model assumes that the rotating current system which creates the rotating magnetic field perturbation is also causing rotating SKR emission at the local time of the upward field-aligned currents (downward going electrons). Using their model of a rotating SKR source we have calculated the SKR phase deviation $\Delta\varphi$ as a function of time from the beginning of 2009 until the end of 2012. Fig. 8 shows the modeled SKR phase deviations calculated for each hour (small black dots), each day (small black stars) and the orbital averaged values over each Cassini orbit (thick black line). The concentration of black stars around certain phase deviations is due to the orbital motion of Cassini. The local time of the spacecraft changes only little around the apoapsis, whereas the spacecraft traverses over large intervals in local time (resulting in large phase deviations) during periapsis passes. SKR observations on a given orbit should be dominated by those around apoapsis where the spacecraft spends most of its time (Andrews et al., 2011).

Fig. 8 shows that there are two intervals of time, when the orbit-averaged phase deviations (thick black line) are changing significantly from orbit to orbit, which are the first half of 2009 and the first half of 2011. These changes are related to shifts of the local time of Cassini apoapsis from ~10 LT (early 2009) to ~19 LT (mid-2009) and from ~18 LT (February 2011) to ~15 LT (mid-2011). As a result, the derived SKR periods of these two time intervals might be not completely correct, but the deviations are not large. For the

Northern SKR intensity vs time and phase (10.63 h)
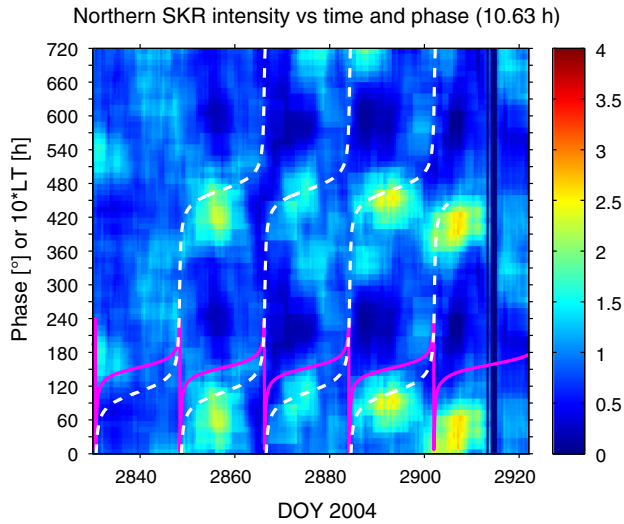
Fig. 9. Normalized northern SKR intensity plotted with respect to a phase with a constant guide period of 10.63 h for late 2011 (October 1 to December 31) showing a rotating SKR signal. This figure is similar to Fig. 3 where the SKR intensity (displayed over two rotations or 720°) is normalized by dividing it by the SKR intensity over one rotation. The magenta line indicates ten times the local time (LT) of the spacecraft with Cassini orbits lasting about 18 days. (The LT in hours can be retrieved by dividing the values at the y-axis of the plot by 10.) The dashed white lines show how a rotating SKR signal would change its phase by 360° over each orbit, and the normalized northern SKR intensity indeed follows closely this trend (The steeper rise of SKR signals at somewhat earlier local times is due to small imperfections of the model which describes the phase deviation as function of spacecraft local time.) (For interpretation of the references to color in this figure legend, the reader is referred to the web version of this article.)

first half of 2009 the SKR phase deviation goes from ~45° at day 1860 to 165° at day 2050 resulting in an average error for the SKR rotation rate of 120°/190 days = 0.6°/day. For the first half of 2011 the changes are from ~140° at day 2600 to ~70° at day 2740, related to an SKR rotation rate error of −70/140 = −0.5°/day. The minus sign for the latter case means that the true SKR rotation rate should be smaller, as a westward movement of the observer (18–15 LT) results in an observed rotation rate which is too fast. Both errors are significantly smaller than the broadness of the SKR signals in the modulation spectra (Figs. 1, 2 and 6) which is typically 2–4°/day. For most of the other time (first half of 2009 and 2011 excluded) Fig. 8 shows that the orbit-averaged phase deviations are roughly constant from one orbit to the next. This actually means that at those times the SKR source can be viewed as being clock-like. Since the rotation rate is the temporal derivative of the phase, a constant shift in phase of the main modulation signals of consecutive Cassini orbits will not result in any change in rotation rate. This can be understood as a second clock, ticking with the same speed as the main clock (when SKR peaks at the morning side, not visible from the apoapsis position of Cassini), but just shifted in phase by the orbit-averaged phase deviation $\Delta\varphi$ shown in Fig. 8. Only when there is a gradient of $\Delta\varphi$, the rotation rates need to be corrected, and we have shown above that these corrections are relatively minor. During the times of constant orbit-averaged phase deviations $\Delta\varphi$ no rotation rate correction is necessary. In essence, the rotational nature of the SKR signal can be obscured, and the SKR *appears* like a clock signal. This can happen not only with Cassini apoapsis on the morning side where the strong morning side SKR sources act clock-like, but also with Cassini apoapsis on the evening side as Fig. 8 shows. The main SKR modulation signals are generally dominated by the observations around apoapsis where there is only little change in Cassini local time.

For a rotating SKR source it should be possible to see the dependence of the SKR phase on the local time of the observer in a phase

plot similar to Fig. 3. In the following Fig. 9 we show the normalized northern SKR intensity versus phase and time for late 2011 (September 20 to December 31). The magenta line indicates ten times the local time of the spacecraft. In contrast to Fig. 3, we have chosen a constant guide period of 10.63 h so that the northern SKR phase should not drift much with time (stay horizontal) corresponding to the northern SKR rotation rate of 813°/day of late 2011. This can clearly be seen as the main SKR intensity is concentrated around 0–120° in phase. There is one large blob of SKR intensity for each orbit, accentuating the fact that the Cassini orbit is modulating the amplitudes of the normalized SKR intensities as mentioned in Section 3. It can be seen in Fig. 9 that the SKR intensities between the blobs are not concentrated around the phase of the main signals (0–120°), but that they extend almost vertically from the edges of the most intense signals. The magenta line in Fig. 9, which is indicating the local time of the observer, shows us that these vertical SKR intensities take place at Cassini periapsis passes (days 2848, 2866, 2884, 2902) when the local time of the spacecraft is changing quickly as well.

The three white lines show how a rotating SKR signal should change its phase just like the observer changes the local time, and indeed the weak, almost vertical SKR signals follow this model quite closely. This can be regarded as a proof that rotating SKR signals do exist, and that the SKR phase can also be position-dependent as suggested by Lamy et al. (2013) and Andrews et al. (2011). Additional rotational signals can be seen in Fig. 7 as will be mentioned in the next subsection. The SKR intensity in Fig. 9 is thus drifting over 360° about every 18-day orbit of Cassini (the last orbit in December 2011 last 24 days). However, our periodicity analysis recognizes mainly the large blobs concentrated in phase around 0–120° which show almost no changing phase since the local time of Cassini only changes slightly around apoapsis. As we have demonstrated with Fig. 8, this means that it is actually the clock-like SKR behavior that is relevant in the periodicity analysis.

5.2. SKR as a clock-like signal

For a clock-like signal, corrections for the position of the observer are not needed, and there is no SKR phase deviation as a function of the observer's local time like in the previous model of the

Southern SKR intensity vs time and subsolar longitude
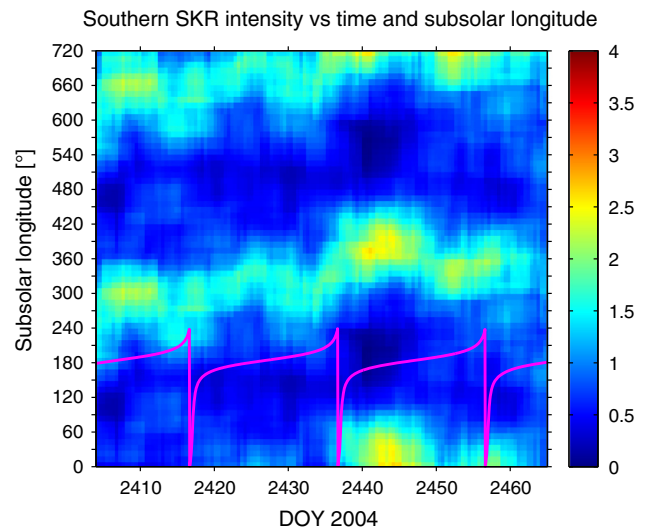
Fig. 10. Normalized southern SKR intensity plotted with respect to Voyager SLS subsolar longitude for August and September 2010. The display is similar to Fig. 9, with the magenta line showing again ten times the local time (LT) of Cassini. The plot goes over 3 Cassini orbits of 20 days each with periapsis passes on days 2417, 2437, and 2457. (For interpretation of the references to color in this figure legend, the reader is referred to the web version of this article.)

rotating signal. In Fig. 10 we have displayed a phase plot (with respect to the Voyager SLS sub-solar longitude) with a strong and continuous SKR signal throughout the displayed time. In contrast to Fig. 9 there are no abrupt phase changes during the large shifts in Cassini local time, only a small shift inconsistent with the predictions of the SKR phase deviation model in Fig. 2c of Andrews et al. (2011) can be seen around the periapsis of day 2437. This behavior is consistent with the classic clock-like signal, similar to the organization of Voyager SKR in a single occurrence peak with sub-solar longitude (Warwick et al., 1981; Gurnett et al., 1981). This means that during the time displayed in Fig. 10, the rotating signals seem not to be present. In Fig. 7, where we organized the normalized northern and southern SKR intensities with respect to a variable period, the main signals at the constant phases around the horizontal dash-dotted lines are due to the clock-like behavior. However, there are also many SKR signals in Fig. 7, which are not in phase with the main clock-like signal. It is likely that most of those signals are due to the rotating SKR source, since most of them show abrupt phase shifts of 360° within one Cassini orbit, similar to the signals of Fig. 9.

The SKR clock can be understood with the camshaft model of Southwood and Kivelson (2009) where a rotating current system produces a signal at a constant local time, which occurs once for each rotation. The rotating SKR signal is thought to be weak except when it reaches the morning side where it intensifies and where it produces the strong clock-like signal. SKR has its largest intensity from sources located in the post-dawn sector peaking around 08 LT (Lamy et al., 2009). The dominance of the clock-like SKR signal would be easy to understand in case SKR would be an isotropic radio source which can be observed from all local times. However, it is well-known that SKR is a beamed radio emission (Cecconi et al., 2009; Lamy et al., 2013) leading to strong visibility effects. The strong clock-like SKR signal from the morning side should practically be invisible with a spacecraft located on the evening side. This makes the dominance of the clock-like SKR signal difficult to understand, since Cassini apoapsis was on the evening to afternoon side after Saturn equinox (e.g. ~18 LT in February 2011) from where the strong morning-side sources are hardly visible. Our analysis of the SKR phase deviation for a rotating SKR source has shown that even rotating signals can *appear* clock-like, albeit with a phase deviation $\Delta\varphi$ with respect to the clock-like signal ($\Delta\varphi = 0°$) displayed in Fig. 8. Our comparison of SKR phases with magnetic oscillation phases in the next section will rather show good agreement at most times and no clear SKR phase deviations. Another possibility would be that at the time of SKR peak amplitude SKR is not only emitted from the strong morning side sources but also from other local times. A careful inspection of Fig. 5a of Lamy (2011) shows that the sources located from 12 to 18 LT appear around the southern SKR maximum phase of $\Phi_S = 0°$ (i.e. no phase deviation), but the data set is rather sparse for the evening side. Further studies, identifying the source regions and phases of the SKR observed by Cassini from the evening side after Saturn equinox, are clearly needed for a better understanding.

In summary, SKR might have both, clock-like sources *and* rotating sources, caused by static and rotating current systems. It is possible that some SKR sources are fixed in local time (Warwick et al., 1981), whilst others are rotating with the aurora (Lamy et al., 2013). One could also imagine SKR sources rotating only over a limited local time range simulating a clock-like behavior. For our tracking-filter analysis we argue that the main modulation signal is due to SKR acting like a clock. We also identified rotating SKR signals in the SKR phase plots of Figs. 9 and 7. It is practically impossible that the major SKR modulation signals are due to the rotating SKR signals, because in that case one would have to apply a rather large correction (360° divided by the orbital duration in days) to all measured SKR rotation rates. The consequence of such

a large correction would be SKR periods largely different to the magnetic field periods, e.g. meaning that the agreement between SKR periods and magnetic field periods before equinox as found by Andrews et al. (2011) would be completely spoiled.

6. Discussion: Differences between SKR and magnetic field rotation rates

6.1. Comparison of rotation rates

In Fig. 11 we compare the rotation rates of SKR and the magnetic field over 4 years from the beginning of 2009 to the end of 2012. The SKR rates have been smoothed by calculating a running average of the values from Fig. 4 over a 60-day window (7 data points). The northern and southern rotation rates derived from the magnetic field oscillations were taken from Table B1 in Provan et al. (2013), and they are plotted in Fig. 11 as blue and red dotted lines with crosses, respectively. In the magnetic field data, Provan et al. (2013) detected abrupt transitions in oscillation period and amplitude in February 2011, August 2011, and April 2012, and they defined corresponding time intervals. E1 was defined as the interval from mid-July 2009 (day 2025), shortly before Saturn equinox, until the first abrupt transition in February 2011. This is followed by interval E2 (February to August 2011, days 2597–2780), E3 (August 2011 to April 2012, days 2780–3018), and E4 (April 2012 to December 2012, days 3018–3259), see Provan et al. (2013) and our Fig. 11. Only a single constant magnetic field period is determined for each hemisphere for the intervals E2, E3, and E4.

It is obvious that there are some differences between the rotation rates derived from the magnetic field and those derived from SKR. There is a relatively good agreement before Saturn equinox as shown by Andrews et al. (2011). For the northern hemisphere, SKR and magnetic period deviate from each other from about days 2070 to 2600 (most of interval E1, end of August 2009 to mid-February 2011) with the magnetic period always being faster than the SKR period. For the southern magnetic and SKR periods of
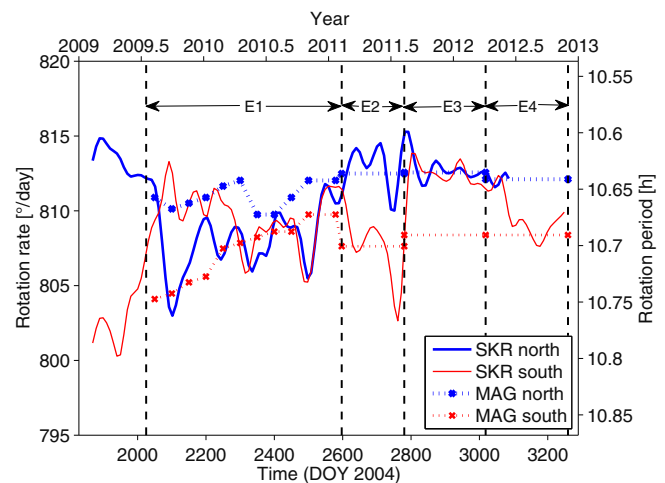
Fig. 11. Comparison of rotation rates (in °/day) of SKR and magnetic field over 4 years from the beginning of 2009 until the end of 2012. The SKR rates of Fig. 4 have been smoothed by calculating a running average over 60 days (7 data points) using a Hamming function as weighting function. They are displayed as solid lines in blue and red color for northern and southern SKR, respectively. For comparison, the rotation rates of the magnetic field (MAG; blue for north, red for south) have been taken from Table B1 of Provan et al. (2013) and are displayed as dotted lines with crosses. The dashed vertical lines separate the time intervals E1, E2, E3, and E4 defined by Provan et al. (2013). The axis on the right side indicates the corresponding rotation period in hours. (For interpretation of the references to color in this figure legend, the reader is referred to the web version of this article.)

interval E1 there is some agreement starting around day 2300 (mid-April 2010). Before that, the southern SKR is much faster, and around the change from 2009 to 2010 it is actually close to the northern magnetic field rate of ~810°/day.

For interval E2, the northern SKR and magnetic periods are within ±2°/day. The southern periods are about equal in the middle and right at the end of interval E2. The northern and southern magnetic periods are not the same at the beginning and the end of interval E2 as it is the case for SKR. The two constant periods derived from the magnetic field data for interval E2 (10.634 h for the north, 10.698 h for the south, Provan et al. (2013)) are not so far from the northern and southern SKR rate. However, a major difference is that SKR rates are changing with time within the interval E2 as is evident in Fig. 11 and from the changing slopes of the SKR phases in Fig. 3.

For time interval E3 the northern magnetic and SKR periods are in good agreement with each other. However, there is a very large deviation (up to 5°/day) between southern magnetic period and southern SKR period, which are only about equal at the beginning of the interval. Provan et al. (2013) determined the phase for each magnetic signal component at every Cassini periapsis pass, and then they followed the phase in their northern and southern format to derive the periods. They used the method of Andrews et al. (2012), which we recall in Appendix D. The phases of the magnetic field can easily be followed for E2 south, E3 north, and E4 north (see Fig. 6 of Provan et al. (2013)), because the signal amplitudes are large in these intervals for the respective hemisphere. But, the phases are much more difficult to follow for the northern signal in interval E2 and for the southern signals in intervals E3 and E4 when oscillation amplitudes are small and magnetic phase values are largely banded. Provan et al. (2013) note that the southern oscillation parameters cannot be reliably determined for interval E3, and only a linear interpolation between the end of E2 and the beginning of E4 was made.

For interval E4 the northern magnetic and SKR periods are similar in the beginning. Fig. 3 shows that we can follow the phase of northern SKR only until day 3085 (mid-June 2012) since the signal is too weak afterwards. Southern SKR and magnetic periods are largely different at the beginning of interval E4, but they reach a similar value in autumn 2012.

6.2. Comparison of SKR to magnetic field phases

So far it was not clear what causes the difference in SKR and magnetic field rotation periods, but we can gain further insight into the problem by comparing the SKR phases to magnetic field phases. The magnetic field phases were determined by Andrews et al. (2011) and Provan et al. (2013) assuming a rotational magnetic field perturbation. Their phases are corrected for the azimuthal motion of the spacecraft (Cowley et al., 2006), whereas no correction is applied to the SKR phases. Our comparison is done in Fig. 12 where the SKR intensities are plotted in a similar way as in Fig. 3, but with different guide periods for both hemispheres and
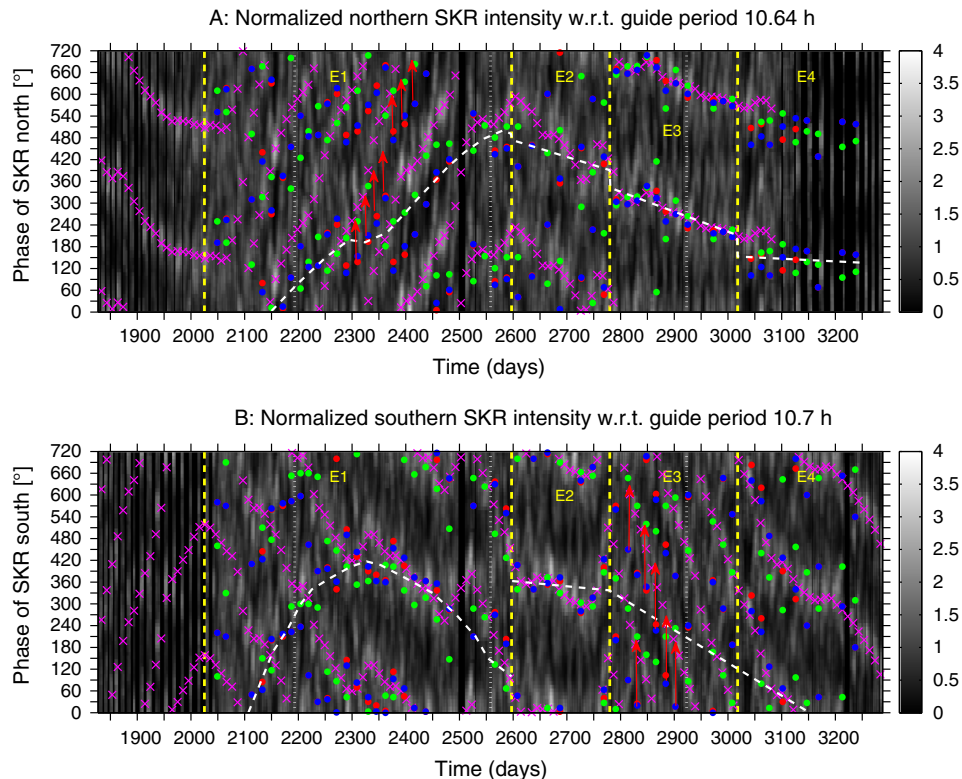
Fig. 12. Comparison of northern and southern SKR and magnetic field phases from the beginning of 2009 until the end of 2012. The SKR phases are drawn similar to Fig. 3, but in gray scaling for a better visibility of the magnetic phase points. The guide periods are 10.64 h for the northern hemisphere (upper panel A), and 10.70 h for the southern hemisphere (lower panel B), similar to Provan et al. (2013). The magenta crosses show the northern and southern SKR phases at the maximum SKR intensity corresponding to the white and red lines of Fig. 3 which trace the SKR maxima. As discussed in the text, the SKR phases were adjusted to bring them to similar phases as the magnetic phases (−90° for northern SKR phases, +90° for southern SKR phases). Panel A shows the magnetic phase data in the northern format for the B_r (red points), B_θ (green points) and the B_φ (blue points) field components. Similarly, red, green and blue points in panel B show the magnetic phase data in southern format for radial, co-latitudinal, and azimuthal magnetic field components. Both northern and southern magnetic phase data (the dots) were phase-shifted from the measured values like in Provan et al. (2013), according to Eqs. (10)–(12) in our Appendix D. The magnetic phase data in northern and southern format were taken from Fig. 6 of Provan et al. (2013), and the dashed white lines indicate the magnetic oscillation phases derived by Provan et al. (2013). The three dotted vertical white lines separate the years. The four dashed yellow lines separate the time intervals E1, E2, E3, and E4 as defined by Provan et al. (2013). The red arrows indicate how phase shifts of +180° (E3, south) or +120° (E1, north) would bring all 3 magnetic phases on one line consistent with the corresponding SKR phase.

in a gray color scale for a better visibility of the magnetic phase points (red, blue and green dots). The guide periods are 10.64 h for the northern hemisphere and 10.70 h for the southern hemisphere, in agreement with the guide periods chosen by Provan et al. (2013). All guide phases of both hemispheres are set to zero at $t = 0$ (January 1, 2004, 00:00 SCET) for SKR and magnetic data. The SKR intensity maxima are traced by the magenta crosses in Fig. 12, and they correspond to the phases of the white and red lines in Fig. 3, but re-calculated to take the new guide periods into account. The positions of the magenta crosses in Fig. 12 can thus be interpreted as the northern and southern SKR phases with respect to the respective guide periods. Those SKR phases are compared to the magnetic phase data, which were taken from Fig. 6 of Provan et al. (2013). The magnetic phases indicated by the red, blue and green dots can be determined for each Cassini periapsis pass for both hemispheres in the so-called northern (N) and southern (S) format by the method of Andrews et al. (2012), which includes subtractions of constant phase angles as we briefly describe it in Appendix D (see Eq. (10)). These subtractions should bring the phases values of the 3 different magnetic components on a common line, denoting the "true" northern and southern magnetic phases ($\Phi_n(t)$ and $\Phi_s(t)$ in Eqs. (11) and (12) in Appendix D) relative to the guide phase employed (Provan et al., 2013). No modifications are done to the phase of the radial component B_r (red dots) such that $\Phi_n(t)$ and $\Phi_s(t)$ correspond by definition to the phases of the northern and southern radial magnetic field components (Andrews et al., 2012). The blue dots are the shifted phase values of the azimuthal B_φ magnetic field component, which are fairly close to the red dots of the radial B_r component. The green dots are the shifted phase values of the co-latitudinal B_θ magnetic field component. In Fig. 12 we also want to bring the SKR phase onto a common line with the 3 magnetic field phases in S-format. According to the model of Andrews et al. (2011) the upward field-aligned current from the ionosphere is expected to be centered ~90° ahead in azimuth of the maximum radial magnetic field component for the southern system. Since upward field-aligned currents correspond to downward going electrons where the corresponding SKR sources should be located, the SKR maximum comes first at smaller guide phases and is then followed by the maximum in the southern B_r component at a larger guide phase. Therefore, we have to add +90° to the southern SKR phase to get on a common line with the 3 southern magnetic field phases in S-format. The situation is the other way round at the northern hemisphere, where the upward field-aligned currents are expected to be 90° behind the northern B_r component (Andrews et al., 2011). Therefore, we subtracted 90° from the northern SKR phase in Fig. 12 to get on a common line with the 3 magnetic components in N-format. A quick look at Fig. 12 shows that these shifts in SKR phases lead to good agreement between magnetic and SKR phases for large intervals of time. This points to a truly clock-like SKR source since the introduction of orbit-averaged SKR phase deviations due to rotating signals as plotted in Fig. 8 would mostly deteriorate the agreement.

The different nature of SKR and magnetic phase data is evident in Fig. 12. The magnetic phases can probably be determined with a higher accuracy (±10° according to Andrews et al. (2012)) compared to the SKR phases where the maxima usually extend over several tens of degrees. However, the magnetic phases oscillate around their true phase, and their deviations from the true phase depend on the phase difference $\Delta\Phi_{MAG}$ and the amplitude ratio k between northern and southern hemisphere (see Appendix D). A clear advantage of the SKR data is its almost continuous presence, whereas magnetic phases can only be determined once at each periapsis pass. This advantage makes a tracing of the phases easier for SKR than for the magnetic data.

We start our detailed comparison of magnetic and SKR phases with the southern hemisphere in Fig. 12B. For interval E1 the agreement looks good starting in spring 2010 (around days 2250–2300) with red, green and blue dots located close to the magenta crosses, which is consistent with similar southern periods as shown in Fig. 11. Only around day 2500 there are some deviations, but the agreement of phases is again okay at the end of interval E1. Large deviations are found from the start of interval E1 until early 2010 when southern magnetic phases and southern SKR phases do not agree with each other. However, there is one remarkable feature, which is the good coincidence of southern SKR phase (magenta crosses) with the magnetic phase of the B_θ component in S-format (green dots) even in the year 2009. Looking ahead one can realize that this coincidence is present throughout the time of Fig. 12 in the southern hemisphere. Interval E2 shows again a good agreement of the shifted SKR phases and the magnetic phases of all S-format components. The tight clustering of the S-format magnetic phases is due to the large amplitude of the southern magnetic field signal (Provan et al., 2013). The good agreement between SKR and magnetic phases suggests that the SKR signals are clock-like or that the model presented in Section 5.1 needs to be modified. The model for the phase deviation of a rotating SKR signal (Fig. 8 in section 5.1) predicts changing phase shifts $\Delta\varphi$ from ~140° to ~70° for interval E2, which are not present in Fig. 12. Fig. 12 also clearly shows that the slope of the southern SKR phase in E2 (i.e. the period) is varying and not constant. This points to the problematic nature of employing piecewise linear fits to the magnetic phase data (dashed white lines in Fig. 12) as done by Provan et al. (2013) resulting in just one period for interval E2, but which is far from what can be seen in Fig. 12B due to the nonlinear behavior. This can result in large errors, much larger than the mathematical errors calculated by Provan et al. (2013) for their linear fits, simply because the assumption of linearity is non-valid. This is especially obvious for the last magnetic phase points of interval E2 which are in perfect agreement with the southern SKR phase which shows a sharp rise within a short time.

For interval E3 Provan et al. (2013) noted the uncertainty of their value for the southern magnetic period due to the small amplitude and the large banding of phases. They only connected the phase values from the end of interval E2 with their supposed phase values at the beginning of interval E4 with a straight line (see their Fig. 6), and their supposed phase value is actually inconsistent with the first measured magnetic phase value of interval E4. As can be seen in our Fig. 12, three full rotations are actually missed with this approach. In interval E3 the SKR phase is in good agreement with the S-format B_θ phase (green dots) whereas the S-format B_r and B_φ phases (red and blue dots) seem to be shifted by ~180°. The arrows in Fig. 12B indicate that such a corrective shift of +180° would indeed lead to an agreement of all S-format magnetic phase values with the southern SKR phase. Such a behavior points to a constant phase difference of $\Delta\Phi_{MAG} = 180°$ between northern and southern magnetic phases as will be shown in Appendix D. We will mathematically demonstrate there that the phase deviation for the S-format B_r and B_φ phases from the true magnetic phase (corrected by the red arrows) should be 180°. A constant phase difference results in similar slopes, i.e. similar periods of both hemispheres. Hence, in our interpretation northern and southern SKR periods as well as northern and southern magnetic field periods all have the same value in interval E3.

In this interpretation SKR and magnetic periods of both hemispheres also have the same value for part of interval E4 until June 2012, after which the northern SKR period cannot be reliably determined anymore. The difference in southern periods at the beginning of interval E4 again results from the calculation of

piecewise linear fits by Provan et al. (2013) whereas the continuous SKR phase data in this interval shows a steep negative slope in the beginning which is slowly getting flatter. The S-format magnetic phase data is actually in agreement with this behavior and the magnetic phase points are banded around the SKR phase. The linear fit of Provan et al. (2013) for interval E4 is far from the first two southern magnetic phase measurements of interval E4 (revs 165 and 166 around day 3050), and similar slopes (periods) are only achieved for the middle of interval E4.

The relation of SKR phases to N and S-format magnetic field phases from equinox to spring 2010 (day 2049–2250) is difficult to interpret and there is almost no agreement. At several periapsis passes the co-latitudinal B_θ phases in N and S-format are close to the northern and southern SKR phase, respectively. However, since the two hemispheric periods are different for both SKR and magnetic field for this time interval, this cannot be interpreted as a case of constant phase difference as before.

Fig. 12A shows general good agreement between northern SKR and magnetic phases, especially for the intervals E2, E3, and E4. In interval E1 from day 2250 to 2450 there is relatively good agreement between the northern SKR phase (magenta crosses) and the N-format B_θ phase (green dots). As shown in Appendix D this could again be interpreted as a constant phase difference $\Delta\Phi_{MAG} = 180°$ between northern and southern magnetic phases. Here the correction for the N-format B_r phase is somewhat smaller, ~120°, which is mathematically justified in Appendix D. This leads again to similar northern and southern magnetic periods just like it is the case for SKR in this time interval. The large difference in northern periods for magnetic field and SKR in E1 thus results from a different tracing of phases. While Provan et al. (2013) assume an oscillation of the N and S-format magnetic phases around the true phase, we suggest an alternate way of tracing the phase simply along the N-format B_θ component phase values which must be employed in case of similar northern and southern periods and a constant phases difference of $\Delta\Phi_{MAG} = 180°$. The mathematical justification for this approach is shown in Appendix D. For the rest of the time Fig. 11 shows a good agreement of northern SKR and magnetic periods from the end of interval E1 (around day 2500) until the beginning of interval E4 (around day 3100). Here all 3 N-format magnetic phases and the shifted northern SKR phase show very good agreement. The northern SKR phase can only be traced until shortly before day 3100 due to the increasingly longer passages of Cassini at higher latitudes through the southern hemisphere.

In summary, there is good agreement between southern SKR phases shifted by +90° and S-format magnetic phases starting from day 2300 (spring 2010) until the end of 2012, if one looks at the relevant magnetic field component (in interval E1 and E3) in case there is a constant phase difference between north and south. Similarly, northern SKR phases shifted by −90° and N-format magnetic phases are also in good agreement. This is in line with the model of Andrews et al. (2011) which expects the northern upward field aligned currents to be 90° behind the northern magnetic radial component, whereas the southern upward currents are leading the southern magnetic radial component by 90°. Thus at the time of southern SKR maxima the upward-field aligned current region should be in the midmorning sector where the most intense SKR sources are located, and at the same time the southern quasi-uniform equatorial magnetic field (the southern radial magnetic field component) points towards the postmidnight sector around 3 LT (Andrews et al., 2011). The similarity between appropriately shifted magnetic and SKR phases combined with a different tracing of magnetic phases as suggested in Appendix D leads to almost complete agreement between magnetic and SKR periods after equinox. Large deviations, which still need to be investigated in more detail, only remain for about half a year from shortly after equinox to spring 2010. The good agreement of SKR and magnetic phases for large intervals of time suggests that the SKR signal is clock-like since the predicted SKR phase deviations for a rotating SKR signal seem not to be present.

7. Conclusions

We have analyzed the rotational modulation of SKR specifically from the beginning of 2009 until the end of 2012. The SKR signal was separated by its wave polarization and by the spacecraft latitude, and we applied a tracking filter analysis technique to analyze the periodicities of northern and southern SKR. We also plotted the phase of normalized northern and southern SKR intensity versus time with respect to a constant guide period. Tracing the phase maxima allows a determination of the rotation rates, and we obtained similar results to the tracking filter analysis technique as illustrated in Fig. 6. We found that the periods of northern and southern SKR crossed in late August 2009, just a few weeks after Saturn equinox, and they coalesced in spring 2010. Most notably, northern and southern SKR periods and phases were similar for almost one year after March 2010 and from August 2011 until June 2012. During the time interval March to July 2011 phases of northern and southern SKR were unlocked again and rotation rates of both hemispheres deviated significantly from each other. We also found rotating SKR signals where the modulation phase deviation amounts one rotation each time Cassini completes one orbit. We compared SKR and magnetic field phases and found that a different tracing of magnetic field phases along single magnetic field component values should be employed in case of constant phase differences between the northern and southern hemisphere. This has led to a good agreement between SKR and magnetic field periods after equinox except for the first half year (equinox to spring 2010).

Appendix A. Tracking filter analysis

The tracking filter analysis (Gurnett et al., 2009a,b, 2011) uses the integrated intensity of the radio waves (integration over 10 min in time and over 200–800 kHz in frequency) as measured by the Cassini Radio and Plasma Wave Science (RPWS) instrument (Gurnett et al., 2004). In the SKR frequency range the channels close to multiples of 100 kHz and the channels at 475 kHz, 643.75 kHz, and 656.25 kHz were excluded from the integration due to interference. The choice of the SKR upper and lower frequency limit of integration is motivated by the fact that SKR covers the frequency range of 200–800 kHz at all local times as Lamy et al. (2008b) have shown in their Fig. 11a. The integrated intensity is then distance-normalized by a division by the average intensity over one Saturn rotation. The resulting normalized intensities are multiplied by a Hanning weighting function with a duration of 240 days. The spectrum analysis is done in 30-day steps leading to a temporal resolution of about 12 measured periods per year. The SKR intensities are then sorted and averaged in 1° longitude bins for a series of assumed rotation rates ranging from 785 to 830°/day. The resulting averages are fit to a sinusoidal function of longitude to determine the peak-to-peak amplitude A. The quantity of $2A^2$ is the normalized peak-to-peak power represented in color in the modulation spectrograms. This periodicity analysis is first applied to the complete SKR signal in Section 2 (Fig. 1), and in Section 3 (Fig. 2) the SKR intensities are separated by spacecraft

latitude and polarization with right-hand polarization attributed to SKR from the northern hemisphere and left-hand polarization to SKR from the southern hemisphere (see Appendix B). In this case the integration over frequency is done for the two separated SKR components, followed by the distance normalization, the multiplication with a Hanning weighting function, and the spectrum analysis separately for both SKR components.

Appendix B. SKR separation by polarization and spacecraft latitude

SKR from both hemispheres (north and south) can reach the RPWS antennas simultaneously leading to an incoherent superposition of oppositely polarized waves. The polarization sense of the superposed waves is the one of the stronger SKR component. Mathematically, the incoherent superposition of two circularly polarized radio waves with intensities S_N and S_S (index N for northern and S for southern intensity) can be written as the sum of two Stokes vectors with the Stokes parameters u, q, v. For completely circularly polarized waves like SKR we have $q_S = u_S = q_N = u_N = 0$ and $v_S = 1$ and $v_N = -1$ yielding the following equation:

$$S_S \begin{pmatrix} 1 \\ q_s \\ u_s \\ v_s \end{pmatrix} + S_N \begin{pmatrix} 1 \\ q_N \\ u_N \\ v_N \end{pmatrix} = S_S \begin{pmatrix} 1 \\ 0 \\ 0 \\ 1 \end{pmatrix} + S_N \begin{pmatrix} 1 \\ 0 \\ 0 \\ -1 \end{pmatrix} = (S_S + S_N) \begin{pmatrix} 1 \\ 0 \\ 0 \\ \frac{S_S - S_N}{S_S + S_N} \end{pmatrix} \tag{1}$$

The last part of Eq. (1) shows that the superposed wave has an intensity of $S = S_S + S_N$ and a degree of circular polarization of $d_c = (S_S - S_N)/(S_S + S_N)$. This means that from our measurement of S and d_c of the superposed signal we can compute the intensity S_N of the northern SKR component and the southern component intensity S_S. Solving the two previous equations for S_S and S_N with simple algebra gives the following two equations:

$$S_S = \frac{S}{2}(1 + d_c), \quad S_N = \frac{S}{2}(1 - d_c) \tag{2}$$

We note that SKR can be elliptically polarized at high latitudes beyond ±30° (Fischer et al., 2009), and therefore Eq. (2) will only be used at lower latitudes where both SKR components (north and south) are completely circularly polarized waves (Lamy et al., 2008b). Also note that the superposition of two completely polarized waves leads to a partially polarized wave with a total polarization degree equal to the circular polarization degree, which is generally less than 1. The separation of SKR is now done by polarization and spacecraft latitude in the following way. For the integration in the frequency range of 200–800 kHz we took only strong SKR with a signal-to-noise ratio larger than 30 (SNR > 30) and, besides the interference channels at multiples of 100 kHz, we also removed data points with a linear polarization larger than 0.9 to further exclude interference. For the absolute value of the circular polarization degree we allowed a range of 0.2–1.1, i.e. $0.2 < |d_c| < 1.1$. This excludes radio emissions with very small circular polarizations, and we allowed absolute values of the circular polarization $|d_c|$ beyond its theoretical maximum of 1.0 due to a typical error for polarization measurements of ~10%. Then we applied a selection criterion with respect to Cassini's latitude and distinguished the following 3 cases:

(1) *High northern latitude above 20°N:* All right-handed (RH) flux fitting the criteria above is integrated and counted as northern flux. The southern flux is set to zero since no southern SKR has been observed at high northern latitudes (Lamy et al., 2008b; Kimura et al., 2013).

(2) *High southern latitudes below 20°S:* All left-handed (LH) flux is southern flux, and the integrated northern flux is set to zero.

(3) *Within ±20° latitude of the equatorial plane:* For all data points fitting the criteria above we used Eq. (2) to calculate northern flux S_N and southern flux S_S for each time/frequency point after which the integration is done separately for northern and southern flux. Due to the errors in polarization measurement resulting from the 8-bit digitization of the receiver we did not count small circular polarizations here. This means that for $d_c > 0.8$ the SKR was considered as a fully LH southern SKR (i.e. $S_S = S$, $S_N = 0$) with no northern flux, and for $d_c < -0.8$ SKR was considered as RH northern flux with no southern flux (i.e. $S_N = S$, $S_S = 0$).

After this separation the SKR intensities of both hemispheres are integrated separately, and the tracking filter analysis described in Appendix A is applied to both of them. This method of separating northern from southern SKR is more precise than a simple separation by the sign of the circular polarization (LH for south, RH for north) since the latter neglects the fact that one time–frequency measurements mostly consists of SKR originating from both hemispheres.

Appendix C. Tracing the phases of SKR maxima

In Fig. 3 we have plotted the normalized intensities of northern and southern SKR from the beginning of 2009 until the end of 2012 with respect to a running guide phase. We used a constant guide period of $\tau_g = 10.6567$ h = 0.44403 d (for both northern and southern SKR; h = hour, d = day), which is arbitrarily chosen as identical to the Voyager radio period of Desch and Kaiser (1981). Thus our guide phase Φ_g is given by

$$\Phi_g = \frac{360°}{\tau_g} t = \omega_g t = 810.7576°/d^t \tag{3}$$

with t as the time in days where we use DOY (day of year) 2004, i.e. $t = 0$ is at 00:00 SCET on January 1, 2004. As mentioned in the caption of Fig. 3, guide phase intervals of 10° (corresponding to 18 min) are taken and the average SKR intensity is calculated in that interval (separately for northern and southern SKR). After normalization for each rotation, the SKR normalized intensities are plotted over two rotations, and in the following we show how the rotation rates can be derived from such a plot like Fig. 3 by tracing the phase of the SKR maximum. The rotation rates of northern and southern SKR (ω_N and ω_S) are varying with time, and they are linked to the SKR phases (Φ_N and Φ_S) by the principal relations

$$\omega_N(t) = \frac{d\Phi_N(t)}{dt}, \quad \omega_S(t) = \frac{d\Phi_S(t)}{dt} \tag{4}$$

The drift of the SKR maximum $\Psi_{N,S}(t)$ with time in each panel of Fig. 3 (northern or southern SKR) is governed by the difference between the guide period and the corresponding SKR period, and for the phases the following relation can be set up:

$$\Psi_{N,S}(t) = \Phi_g(t) - \Phi_{N,S}(t) \tag{5}$$

Using Eqs. (5) and (3) one can calculate the rotation rates of northern and southern SKR in the following way:

$$\omega_N = \frac{d\Phi_N}{dt} = \frac{d}{dt}(\Phi_g(t) - \Psi_N(t)) = \omega_g - \frac{d\Psi_N(t)}{dt} \tag{6}$$

$$\omega_S = \frac{d\Phi_S}{dt} = \frac{d}{dt}(\Phi_g(t) - \Psi_S(t)) = \omega_g - \frac{d\Psi_S(t)}{dt} \tag{7}$$

Eq. (6) tells us that the rotation rate of northern SKR can be derived from the slope of the line $\Psi_N(t)$ that traces the northern SKR

maximum in the phase plot of Fig. 3. If the slope $d\Psi_N(t)/dt$ equals zero then the northern SKR rotation rate/period equals the guide rate/period ($\omega_N = \omega_g$ and $\tau_N = \tau_g$). A positive slope $d\Psi_N(t)/dt > 0$ means a smaller rotation rate (longer period) of northern SKR compared to the guide rate/period ($\omega_N < \omega_g$ and $\tau_N > \tau_g$). Conversely, a negative slope $d\Psi_N(t)/dt < 0$ of the line tracing the northern SKR maximum stands for a faster rotation (shorter period) of northern SKR compared to the guide ($\omega_N > \omega_g$ and $\tau_N < \tau_g$). The phase on the ordinate axes of Fig. 3 is analogous to a westward longitude system where, seen from a fixed position in local time, the longitude is increasing with time. A decreasing guide phase difference (negative slope) can then be understood like a decreasing western longitude or an eastward drift which means a faster rotation. Similarly, an increasing guide phase difference (positive slope) is analogous to a westward drift or a slower rotation period since Saturn rotates eastward.

We note that we did not include a time correction taking into account the finite propagation speed of radio waves from the SKR sources close to Saturn to the Cassini spacecraft. The maximum distance of Cassini to Saturn in the years 2009–2012 was around $68R_S$ (Saturn radii), and SKR propagating with the speed of light would need mere 14 s to propagate this distance. Since our guide period is 10.6567 h corresponding to a full rotation of 360°, a delay time of 14 s corresponds to an angular shift of just 0.13°. Such a small shift is negligible in our Fig. 3 where the normalized SKR intensities are plotted with an angular resolution of 10°.

In Fig. 3 we also traced the SKR maxima by magenta stars in a mathematical way in a procedure of directional statistics which we describe here. The normalized SKR intensities can be plotted radially in a polar diagram depending on the SKR phase angle, and the procedure aims to find the average "direction" (i.e. phase in degrees) where the main SKR intensities are concentrated. A similar method has been employed by Andrews et al. (2011) for tracing the magnetic phases after the methods described in Mardia and Jupp (2000). For each hemisphere Fig. 3 displays a 2D-matrix A_{ij} with a size of 36 × 3292 of normalized SKR intensity values (color scale). The number of rows i represents the number of phase values, where we have 36 values with 10° resolution spanning one full rotation of 360°. The number of columns j is the number of Saturn rotations with the guide period over 4 years. Now we calculate the following double sums:

$$\bar{x} = \sum_{ij} A_{ij} \cos \varphi_i \quad \text{and} \quad \bar{y} = \sum_{ij} A_{ij} \sin \varphi_i \tag{8}$$

The summation over i goes over 36 values and φ_i runs from 5° to 355° in 10° steps. For the summation over j we have chosen 61 rotations (about 27 days), 30 rotations prior to the central rotation and 30 rotations afterwards. The choice of this value determines the time interval over which the directional statistic is done. The average angle around which the normalized SKR intensities A_{ij} are concentrated is now given by

$$\bar{\varphi} = \tan^{-1} \frac{\bar{y}}{\bar{x}} \tag{9}$$

where the inverse tangent function has to be the four-quadrant arc tangent. This average angle is now plotted as a magenta star in Fig. 3 at the time of the central rotation. We repeated this procedure every 22 Saturn rotations to place one magenta star about every 10 days. We also note that the existence of other SKR signals around the main normalized SKR maxima (e.g. from rotating SKR sources) has an influence on the directional statistics and leads to deviations and fluctuations around the SKR maxima. It is for this reason that the white and red lines tracing the SKR maxima in Fig. 3 were drawn by hand, but guided by the results of the directional statistics.

Appendix D. Remarks to the method of Andrews et al. (2012)

The method of Andrews et al. (2012) is a sophisticated method to derive the oscillation phases and periods of the northern and southern magnetic field perturbations. For regions close to the equatorial plane the perturbation field is assumed to be quasi-uniform, with one quasi-uniform field rotating in the southern hemisphere with the southern period and another quasi-uniform field in the northern hemisphere rotating with the northern period (see Fig. 1 of Andrews et al. (2012)). The magnetic perturbation field (gained by subtraction of the internal planetary field and after band-pass filtering) is divided into radial (r), azimuthal (φ), and co-latitudinal (θ) components named B_r, B_φ, and B_θ. There are fixed phase angles between those 3 components in the two (northern and southern) systems, which are given by the following equations (Andrews et al., 2012):

$$\begin{aligned} \gamma_{rs} &= \gamma_{rn} = 0° \\ \gamma_{\varphi s} &= \gamma_{\varphi n} = 90° \\ \gamma_{\theta s} &= 0°, \quad \gamma_{\theta n} = 180° \end{aligned} \tag{10}$$

The phase angles of the radial (r) components are defined to be identical to zero, and both northern and southern azimuthal (φ) components are in lagging quadrature (90°) to the radial component. In the southern system the co-latitudinal component (θ) is in phase with the radial component, but for the northern system it is in anti-phase. These fixed phase angles are subtracted from $\Psi_i(t)$ ($i = r$, φ, θ) which represent the phases determined by the Cassini magnetometer from pass to pass over time (for details see Andrews et al. (2012) or Provan et al. (2013)). The in-situ magnetic field measurements comprise the magnetic perturbations in a "core region" up to a distance of $12R_S$ (Saturn radii). The following two equations are valid for the so-called northern and southern format, respectively (Eqs. (3d) and (3e) of Provan et al. (2013)):

$$\Psi_i(t) - \gamma_{in} = \Phi_{gn}(t) - \Phi_n(t) + \delta_{in}(t) \tag{11}$$

$$\Psi_i(t) - \gamma_{is} = \Phi_{gs}(t) - \Phi_s(t) + \delta_{is}(t) \tag{12}$$

The left-hand side of Eq. (11) represents the phase data of the three magnetic field components, such that for oscillations dominated by the northern system all the phase values lie on a common line denoting the northern magnetic phase $\Phi_n(t)$ relative to the northern guide phase $\Phi_{gn}(t)$ which is employed (Provan et al., 2013). The same holds for the southern system in the similar Eq. (12) where a southern guide phase $\Phi_{gs}(t)$ is used. The phases on the left hand side of both equations are plotted versus time (N-format and S-format diagrams like in Fig. 6 of Provan et al. (2013)), and suitable fits are made with the phase data to derive the "true" magnetic phases $\Phi_n(t)$ and $\Phi_s(t)$ since both guide phases (10.64 h and 10.70 h were used as guide periods) are known. However, there is a little difficulty coming from phase deviations (named $\delta_{in}(t)$ and $\delta_{is}(t)$) resulting from the beating of signals of close frequencies. The size of these deviations determines the banding of the phase values around the true magnetic phase, and Provan et al. (2013) note that in case of equal northern and southern amplitudes the N-format phase values raster through ±90° about $\Phi_{gn}(t) - \Phi_n(t)$, and similarly the S-format phase values raster through ±90° about $\Phi_{gs}(t) - \Phi_s(t)$. The phase deviations $\delta_{in}(t)$ and $\delta_{is}(t)$ depend on the phase difference (beat phase) $\Delta\Phi_{MAG}(t) = \Phi_n(t) - \Phi_s(t)$ between northern and southern magnetic phases, and on the amplitude ratio k of northern magnetic to southern magnetic amplitude. The following equations were derived by Andrews et al. (2012):

$$\delta_{rn}(t) = \delta_{\varphi n}(t) = \tan^{-1}\left[\frac{\left(\frac{1}{k}\right)\sin\Delta\Phi}{1 + \left(\frac{1}{k}\right)\cos\Delta\Phi}\right] \tag{13a}$$
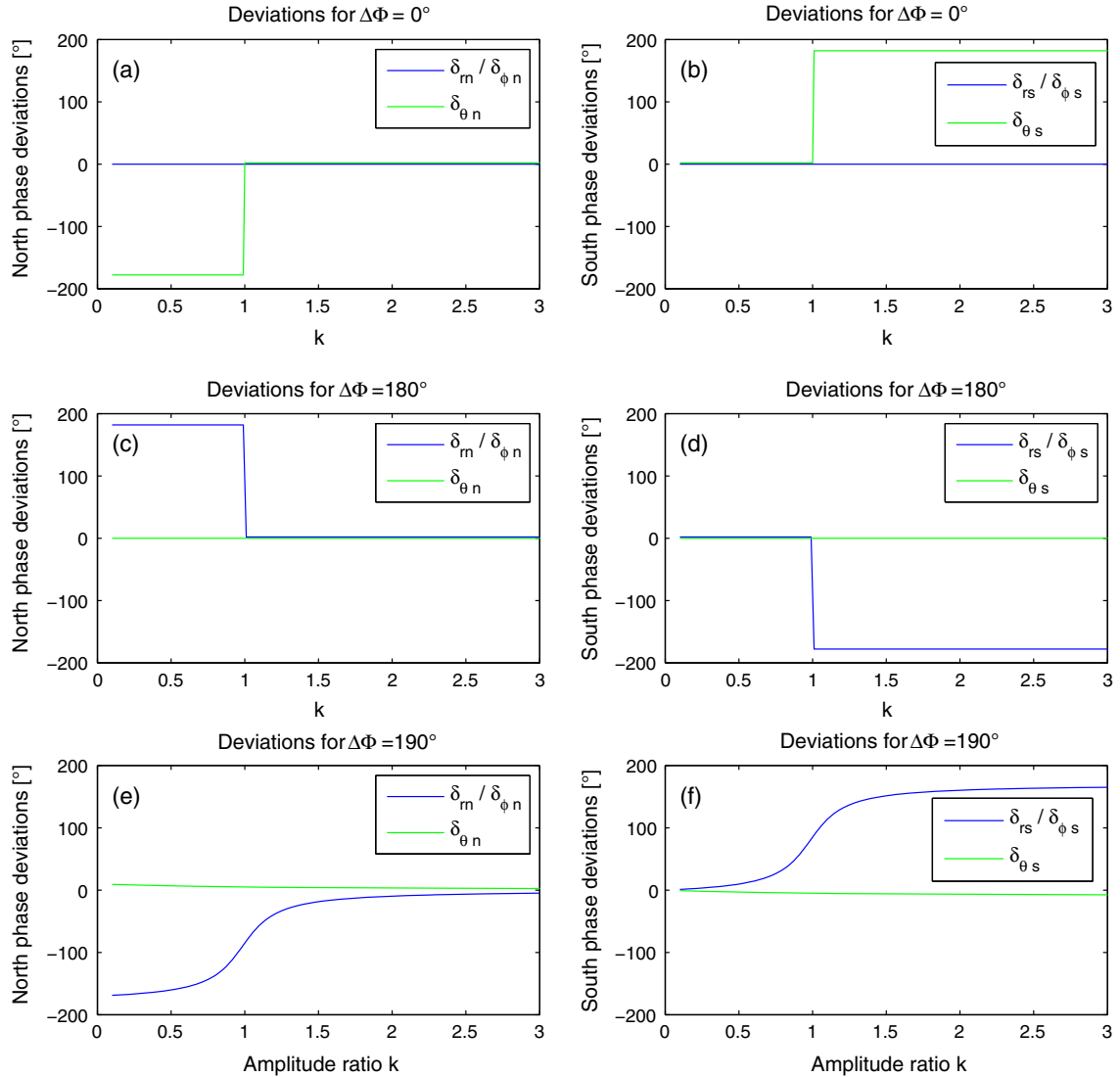
Fig. 13. Calculations of magnetic phase deviations as a function of amplitude ratio k for 3 constant phase deviations $\Delta\Phi_{MAG}$ after Eq. (13). The deviations from the true northern magnetic phase δ_{in} ($i = r, \theta, \varphi$) are displayed on the left side in panels (a), (c), and (e). The deviations from the true southern magnetic phase δ_{is} are on the right in panels (b), (d), and (f). The phase deviations are the same for the radial (r) and azimuthal (φ) magnetic field component (blue lines), and the phase deviations from the co-latitudinal (θ) magnetic field component are drawn as green lines. (For interpretation of the references to color in this figure legend, the reader is referred to the web version of this article.)

$$\delta_{\theta n}(t) = \tan^{-1}\left[\frac{-\left(\frac{1}{k}\right)\sin\Delta\Phi}{1 - \left(\frac{1}{k}\right)\cos\Delta\Phi}\right] \tag{13b}$$

$$\delta_{rs}(t) = \delta_{\varphi s}(t) = \tan^{-1}\left[\frac{-k\sin\Delta\Phi}{1 + k\cos\Delta\Phi}\right] \tag{13c}$$

$$\delta_{\theta s}(t) = \tan^{-1}\left[\frac{k\sin\Delta\Phi}{1 - k\cos\Delta\Phi}\right] \tag{13d}$$

Eqs. (13a) and (13b) describe the phase deviations from the true northern phase, and similarly Eqs. (13c) and (13d) give the southern phase deviations (the inverse tangent function has to be the four-quadrant arctangent). In both hemispheres the deviation of the radial component phase is the same as for the azimuthal component phase. All Eq. (13) have been plotted by Provan et al. (2013) (see their Fig. 2) for 3 different constant values of $k = 0.5$, 1, 2 as a function of the phase difference $\Delta\Phi_{MAG}(t)$, describing the phase deviations as a result of beating signals as a function of time. There it is clearly shown that e.g. for $k = 1$ the phase deviations

oscillate by ±90° around the true phase with changing $\Delta\Phi_{MAG}(t)$ as mentioned above. In Section 4 we have shown that SKR northern and southern periods and phases are similar (i.e. $\Delta\Phi_{SKR} = const.$) over extended periods of time after equinox. Therefore, we take a different approach here and plot the phase deviations as a function of the amplitude ratio k for 3 different constant phase differences of $\Delta\Phi_{MAG} = 0°$, 180°, 190° in Fig. 13, i.e. for the special case of the same northern and southern period. For the same northern and southern magnetic phase ($\Delta\Phi_{MAG} = 0°$) we find that $\delta_{rn} = \delta_{\varphi n} = \delta_{rs} = \delta_{\varphi s} = 0°$ (see panels (a) and (b) of Fig. 13). This means that the radial and azimuthal magnetic phases are actually showing the true northern and southern magnetic phase regardless of the amplitude ratio k. The co-latitudinal component shows a phase deviation of $\delta_{\theta s} = +180°$ for $k > 1$ or $\delta_{\theta n} = -180°$ for $k < 1$.

We recall the situation which concerns time interval E3, when the southern co-latitudinal phase value (green dots in Fig. 12B) were following the southern SKR phase very closely whereas the radial and azimuthal phase values (red and blue dots in Fig. 12B) were shifted in phase by about 180°. For interval E3 we found a constant $\Delta\Phi_{SKR}$ of zero, and magnetic data indicates a northern

dominance with $k > 1$. This situation can be perfectly explained by a magnetic phase difference of $\Delta\Phi_{MAG} = 180°$ as is shown in Fig. 13d which results in no phase shift for the co-latitudinal phase component (green line) and a phase deviation of $-180°$ for the radial and azimuthal phase components for $k > 1$ (blue line). This is exactly what can be seen in Fig. 12B for interval E3. A correction of this deviation by $+180°$ (for radial and azimuthal components) yields three magnetic field components on the same line with the southern SKR phase (see red arrows in Fig. 12B). For the northern hemisphere all components indicate the true northern phase for $k > 1$ as Fig. 13c shows. The interpretation is that northern and southern SKR and northern and southern magnetic field all have the same period in interval E3. Northern and southern SKR phases are actually the same for interval E3 (see Fig. 5), but in Fig. 12 they have been plotted with a phase difference of 180° between them (northern SKR phase shifted by $-90°$, southern SKR phase shifted by $+90°$). This signifies that the difference between true northern and true southern magnetic phase is indeed $\Delta\Phi_{MAG} = 180°$. The situation of $\Delta\Phi_{MAG} = 180°$ is illustrated in Fig. 1 of Andrews et al. (2011) showing the directions of the effective centered transverse dipoles corresponding to the magnetic perturbation fields by two solid arrows, the green one for the northern hemisphere pointing sunward, and the red one for the southern hemisphere pointing in anti-sunward direction, in anti-phase to the green one. This configuration has upward currents on the dawn side for both northern and southern hemisphere, which causes SKR on the dawn side in both hemispheres with a phase difference of $\Delta\Phi_{SKR} = 0°$.

Similar considerations are also valid for parts of interval E1, when the northern SKR phase is consistent with the phase of the N-format co-latitudinal magnetic field component B_θ. However, in that case Fig. 12A shows that the N-format phases of B_r and B_φ are not shifted by exactly 180° with respect to the true magnetic phase, but by somewhat less ~120°. This reduced shift can be easily explained by the fact that the amplitude ratio k is around 1 for interval E1 (Provan et al., 2013) and that $\Delta\Phi_{MAG}$ might not be exactly 180°. This is illustrated in Fig. 13e where a phase difference of $\Delta\Phi_{MAG} = 190°$ leads to phase deviations $\delta_{rn} = \delta_{\varphi n} \approx -100°$ for $k \approx 1$ whereas $\delta_{\theta n}$ is still close to zero regardless of amplitude ratio k.

These calculations have shown that fits to the magnetic field phases are indeed a delicate issue, which can lead to inconsistent magnetic and SKR periods if it is assumed that all the magnetic phases are oscillating around their true phases. Here we have shown that for the important exception of constant phase differences $\Delta\Phi_{MAG}$ of 0° or 180° the measured magnetic phases are not oscillating around the true magnetic phase, but only the phases of single N or S-format field components (B_r, B_φ for $\Delta\Phi_{MAG} = 0°$, B_θ for $\Delta\Phi_{MAG} = 180°$) are identical to the true magnetic phase regardless of the amplitude ratio k. This second possibility of tracing magnetic phases, which was not considered in Andrews et al. (2012) or Provan et al. (2013), leads to consistent magnetic and SKR periods in parts of time interval E1 and in the complete interval E3. In retrospect it is understandable why northern and southern magnetic periods of Provan et al. (2013) never coalesced. Not taking the intricate behavior of magnetic phases for constant phase differences into account means to a priori exclude the possibility of coalescing periods.

References

Andrews, D.J. et al., 2008. Planetary period oscillations in Saturn's magnetosphere: Phase relation of equatorial magnetic field oscillations and Saturn kilometric radiation modulation. J. Geophys. Res. 113, A09205. http://dx.doi.org/10.1029/2007JA012937.

Andrews, D.J. et al., 2011. Planetary period oscillations in Saturn's magnetosphere: Evidence in magnetic field phase data for rotational modulation of Saturn kilometric radiation emissions. J. Geophys. Res. 116, A09206. http://dx.doi.org/10.1029/2011JA016636.

Andrews, D.J. et al., 2012. Planetary period oscillations in Saturn's magnetosphere: Evolution of magnetic oscillation properties from southern summer to post-equinox. J. Geophys. Res. 117, A04224. http://dx.doi.org/10.1029/2011JA017444.

Badman, S.V. et al., 2013. Bursty magnetic reconnection at Saturn's magnetopause. Geophys. Res. Lett. 40, 1027–1031. http://dx.doi.org/10.1002/grl.50199.

Bunce, E.J. et al., 2014. Cassini nightside observations of the oscillatory motion of Saturn's northern auroral oval. J. Geophys. Res. 119, 3528–3543. http://dx.doi.org/10.1002/2013JA019527.

Carbary, J.F. et al., 2009. Dual periodicities in energetic electrons at Saturn. Geophys. Res. Lett. 36, L20103. http://dx.doi.org/10.1029/2009GL040517.

Carbary, J.F. et al., 2011. Post-equinox periodicities in Saturn's energetic electrons. Geophys. Res. Lett. 38, L24104. http://dx.doi.org/10.1029/2011GL050259.

Cecconi, B. et al., 2009. Goniopolarimetric study of the revolution 29 perikrone using the Cassini Radio and Plasma Wave Science instrument high-frequency radio receiver. J. Geophys. Res. 114, A03215. http://dx.doi.org/10.1029/2008JA013830.

Cowley, S.W.H. et al., 2006. Cassini observations of planetary-period magnetic field oscillations in Saturn's magnetosphere: Doppler shifts and phase motion. Geophys. Res. Lett. 33, L07104. http://dx.doi.org/10.1029/2005GL025522.

Davies, M.E. et al., 1996. Report of the IAU/COSPAR working group on cartographic coordinates and rotational elements of the planets and satellites: 1994. Celest. Mech. Dynam. Astron. 63, 127–148. http://dx.doi.org/10.1007/BF00693410.

Desch, M.D., Kaiser, M.L., 1981. Voyager measurements of the rotation period of Saturn's magnetic field. Geophys. Res. Lett. 8, 253–256. http://dx.doi.org/10.1029/GL008i003p00253.

Espinosa, S.A., Dougherty, M.K., 2000. Periodic perturbations in Saturn's magnetic field. Geophys. Res. Lett. 27, 2785–2788. http://dx.doi.org/10.1029/2000GL000048.

Espinosa, S.A., Southwood, D.J., Dougherty, M.K., 2003a. Reanalysis of Saturn's magnetospheric field data view of spin-periodic perturbations. J. Geophys. Res. 108 (A2), 1085. http://dx.doi.org/10.1029/2001JA005083.

Espinosa, S.A., Southwood, D.J., Dougherty, M.K., 2003b. How can Saturn impose its rotation period in a noncorotating magnetosphere? J. Geophys. Res. 108 (A2), 1086. http://dx.doi.org/10.1029/2001JA005084.

Fischer, G. et al., 2009. Elliptical polarization of Saturn kilometric radiation observed from high latitude. J. Geophys. Res. 114, A08216. http://dx.doi.org/10.1029/2009JA014176.

Fischer, G. et al., 2011. A giant thunderstorm on Saturn. Nature 475, 75–77. http://dx.doi.org/10.1038/nature10205.

Fischer, G. et al., 2014. A possible influence of the Great White Spot on Saturn kilometric radiation periodicity. Ann. Geophys. 32, 1463–1476. http://dx.doi.org/10.5194/angeo-32-1463-2014.

Galopeau, P., Lecacheux, A., 2000. Variations of Saturn's radio rotation period measured at kilometer wavelengths. J. Geophys. Res. 105, 13089–13101. http://dx.doi.org/10.1029/1999JA005089.

Goldreich, P., Farmer, A.J., 2007. Spontaneous axisymmetry breaking of the external magnetic field at Saturn. J. Geophys. Res. 112, A05225. http://dx.doi.org/10.1029/2006JA012163.

Gurnett, D.A., Kurth, W.S., Scarf, F.L., 1981. Plasma waves near Saturn – Initial results from Voyager 1. Science 212, 235–239.

Gurnett, D.A. et al., 2004. The Cassini Radio and Plasma Wave investigation. Space Sci. Rev. 114, 395–463. http://dx.doi.org/10.1007/s11214-004-1434-0.

Gurnett, D.A. et al., 2005. Radio and plasma wave observations at Saturn from Cassini's approach and first orbit. Science 307, 1255–1259.

Gurnett, D.A. et al., 2007. The variable rotation period of the inner region of Saturn's plasma disk. Science 316, 442–445. http://dx.doi.org/10.1126/science.1138562.

Gurnett, D.A. et al., 2009a. Discovery of a north–south asymmetry in Saturn's radio rotation period. Geophys. Res. Lett. 36, L16102. http://dx.doi.org/10.1029/2009GL039621.

Gurnett, D.A. et al., 2009b. A north–south difference in the rotation rate of auroral hiss at Saturn: Comparison to Saturn's kilometric radio emission. Geophys. Res. Lett. 36, L21108. http://dx.doi.org/10.1029/2009GL040774.

Gurnett, D.A. et al., 2010. The reversal of the rotational modulation rates of the north and south components of Saturn kilometric radiation near equinox. Geophys. Res. Lett. 37, L24101. http://dx.doi.org/10.1029/2010GL045796.

Gurnett, D.A. et al., 2011. An SLS4 longitude system based on a tracking filter analysis of the rotational modulation of Saturn kilometric radiation. In: Rucker, H.O., Kurth, W.S., Louarn, P., Fischer, G. (Eds.), Planetary Radio Emissions VII. Austrian Academy of Sciences Press, Vienna, pp. 51–64.

Huang, T.S., Hill, T.W., 1989. Corotation lag of the jovian atmosphere, ionosphere, and magnetosphere. J. Geophys. Res. 94, 3761–3765. http://dx.doi.org/10.1029/JA094iA04p03761.

Jia, X., Kivelson, M.G., 2012. Driving Saturn's magnetospheric periodicities from the upper atmosphere/ionosphere: Magnetotail response to dual sources. J. Geophys. Res. 117, A11219. http://dx.doi.org/10.1029/2012JA018183.

Jia, X., Kivelson, M.G., Gombosi, T.I., 2012. Driving Saturn's magnetospheric periodicities from the upper atmosphere/ionosphere. J. Geophys. Res. 117, A04215. http://dx.doi.org/10.1029/2011JA017367.

Kaiser, M.L. et al., 1980. Voyager detection of nonthermal radio emission from Saturn. Science 209, 1238–1240.

Kaiser, M.L. et al., 1984. Saturn as a radio source. In: Gehrels, T., Matthews, M.S. (Eds.), Saturn. Univ. Arizona Press, Tuscon, pp. 378–415.

Khurana, K.K. et al., 2009. Sources of rotational signals in Saturn's magnetosphere. J. Geophys. Res. 114, A02211. http://dx.doi.org/10.1029/2008JA013312.

Kimura, T. et al., 2013. Long-term modulations of Saturn's auroral radio emissions by the solar wind and seasonal variations controlled by the solar ultraviolet flux. J. Geophys. Res. 118, 7019–7035. http://dx.doi.org/10.1002/2013JA018833.

Kurth, W.S. et al., 2007. A saturnian longitude system based on a variable kilometric radiation period. Geophys. Res. Lett. 34, L02201. http://dx.doi.org/10.1029/2006GL028336.

Kurth, W.S. et al., 2008. An update to a saturnian longitude system based on kilometric radio emissions. J. Geophys. Res. 113, A05222. http://dx.doi.org/10.1029/2007JA012861.

Lamy, L., 2011. Variability of southern and northern SKR periodicities. In: Rucker, H.O., Kurth, W.S., Louarn, P., Fischer, G. (Eds.), Planetary Radio Emissions VII. Austrian Academy of Sciences Press, Vienna, pp. 39–50.

Lamy, L. et al., 2008a. Modeling of Saturn kilometric radiation arcs and equatorial shadow zone. J. Geophys. Res. 113, A10213. http://dx.doi.org/10.1029/2008JA013464.

Lamy, L. et al., 2008b. Saturn kilometric radiation: Average statistical properties. J. Geophys. Res. 113, A07201. http://dx.doi.org/10.1029/2007JA012900.

Lamy, L. et al., 2009. An auroral oval at the footprint of Saturn's kilometric radio sources, collocated with the UV aurorae. J. Geophys. Res. 114, A10212. http://dx.doi.org/10.1029/2009JA014401.

Lamy, L. et al., 2011. Emission and propagation of Saturn kilometric radiation: Magnetoionic modes, beaming pattern, and polarization state. J. Geophys. Res. 116, A04212. http://dx.doi.org/10.1029/2010JA016195.

Lamy, L. et al., 2013. Multispectral simultaneous diagnosis of Saturn's aurorae throughout a planetary rotation. J. Geophys. Res. 118, 4817–4843. http://dx.doi.org/10.1002/jgra.50404.

Mardia, K.V., Jupp, P.E., 2000. Directional Statistics. Wiley, Chichester, UK.

Nichols, J.D. et al., 2008. The oscillations of Saturn's southern auroral oval. J. Geophys. Res. 113, A11205. http://dx.doi.org/10.1029/2008JA013444.

Paranicas, C. et al., 2005. Periodic intensity variations in global ENA emissions of Saturn. Geophys. Res. Lett. 32, L21101. http://dx.doi.org/10.1029/2005GL023656.

Provan, G. et al., 2013. Planetary period magnetic field oscillations in Saturn's magnetosphere: Postequinox abrupt nonmonotonic transitions to northern system dominance. J. Geophys. Res. 118, 3243–3264. http://dx.doi.org/10.1002/jgra.50186.

Sánchez-Lavega, A. et al., 2011. Deep winds beneath Saturn's upper clouds from a seasonal long-lived planetary-scale storm. Nature 475, 71–74. http://dx.doi.org/10.1038/nature10203.

Sayanagi, K.M. et al., 2013. Dynamics of Saturn's great storm of 2010–2011 from Cassini ISS and RPWS. Icarus 223, 460–478. http://dx.doi.org/10.1016/j.icarus.2012.12.013.

Smith, C.G.A., 2006. Periodic modulation of gas giant magnetospheres by the neutral upper atmosphere. Ann. Geophys. 24, 2709–2717. http://dx.doi.org/10.5194/angeo-24-2709-2006.

Smith, C.G.A., 2014. On the nature and location of the proposed twin vortex systems in Saturn's polar upper atmosphere. J. Geophys. Res. 119, 5964–5977. http://dx.doi.org/10.1002/2014JA019934.

Southwood, D.J., Kivelson, M.G., 2009. The source of Saturn's periodic radio emission. J. Geophys. Res. 114, A09201. http://dx.doi.org/10.1029/2008JA013800.

Warwick, J.W. et al., 1981. Planetary radio astronomy observations from Voyager 1 near Saturn. Science 212, 239–243.

Ye, S.-Y. et al., 2010. Dual periodicities in the rotational modulation of Saturn narrowband emissions. J. Geophys. Res. 115, A12258. http://dx.doi.org/10.1029/2010JA015780.

Zarka, P. et al., 2007. Modulation of Saturn's radio clock by solar wind speed. Nature 450, 265–267. http://dx.doi.org/10.1038/nature06237.